5-25-2006

Towards a Microscopic Model of Magnetoelectric Interactions in $Ni_3V_2O_8$

A. Brooks Harris
University of Pennsylvania, harris@sas.upenn.edu

Taner Yildirim
University of Pennsylvania, taner@seas.upenn.edu

Amnon Aharony

Ora Entin-Wohlman

Recommended Citation

Harris, A., Yildirim, T., Aharony, A., & Entin-Wohlman, O. (2006). Towards a Microscopic Model of Magnetoelectric Interactions in $Ni_3V_2O_8$. *Physical Review B, 73* 184433-1-184433-16. http://dx.doi.org/10.1103/PhysRevB.73.184433

At the time of publication, author Taner Yildirim was affiliated with the National Institute of Standards and Technology, Gaithersburg, Maryland. Currently, he is a faculty member in the Materials Science and Engineering Department at the University of Pennsylvania.

Towards a Microscopic Model of Magnetoelectric Interactions in $Ni_3V_2O_8$

Abstract
We develop a microscopic magnetoelectric coupling in $Ni_3V_2O_8$ (NVO) which gives rise to the trilinear phenomenological coupling used previously to explain the phase transition in which magnetic and ferroelectric order parameters appear simultaneously. Using combined neutron scattering measurements and first-principles calculations of the phonons in NVO, we identify eleven phonons which can induce the observed spontaneous polarization. A few of these phonons can actually induce a significant dipole moment. Using the calculated atomic charges, we find that the required distortion to induce the observed dipole moment is very small (~0.001Å) and therefore it would be very difficult to observe the distortion by neutron-powder diffraction. Finally, we identify the derivatives of the exchange tensor with respect to atomic displacements, which are needed for a microscopic model of a spin-phonon coupling in NVO. We also analyze two toy models to illustrate that although the Dzyaloshinskii-Moriya interaction is often very important for coexisting of magnetic and ferroelectric order, it is not the only mechanism when the local site symmetry of the system is low enough. In fact, this coexistence can arise in NVO only due to the symmetric exchange anisotropies.

Disciplines
Physics | Quantum Physics

Comments
At the time of publication, author Taner Yildirim was affiliated with the National Institute of Standards and Technology, Gaithersburg, Maryland. Currently, he is a faculty member in the Materials Science and Engineering Department at the University of Pennsylvania.

Towards a microscopic model of magnetoelectric interactions in $Ni_3V_2O_8$

A. B. Harris,[1] T. Yildirim,[2] A. Aharony,[3,4] and O. Entin-Wohlman[3,4]
[1]*Department of Physics and Astronomy, University of Pennsylvania, Philadelphia, Pennsylvania 19104, USA*
[2]*NIST Center for Neutron Research, National Institute of Standards and Technology, Gaithersburg, Maryland 20899, USA*
[3]*School of Physics and Astronomy, Raymond and Beverly Sackler Faculty of Exact Sciences, Tel Aviv University, Tel Aviv 69978, Israel*
[4]*Department of Physics, Ben Gurion University of the Negev, Beer Sheva 84105, Israel*
(Received 1 November 2005; revised manuscript received 23 March 2006; published 25 May 2006)

We develop a microscopic magnetoelectric coupling in $Ni_3V_2O_8$ (NVO) which gives rise to the trilinear phenomenological coupling used previously to explain the phase transition in which magnetic and ferroelectric order parameters appear simultaneously. Using combined neutron scattering measurements and first-principles calculations of the phonons in NVO, we identify eleven phonons which can induce the observed spontaneous polarization. A few of these phonons can actually induce a significant dipole moment. Using the calculated atomic charges, we find that the required distortion to induce the observed dipole moment is very small ($\sim$0.001 Å) and therefore it would be very difficult to observe the distortion by neutron-powder diffraction. Finally, we identify the derivatives of the exchange tensor with respect to atomic displacements, which are needed for a microscopic model of a spin-phonon coupling in NVO. We also analyze two toy models to illustrate that although the Dzyaloshinskii-Moriya interaction is often very important for coexisting of magnetic and ferroelectric order, it is not the only mechanism when the local site symmetry of the system is low enough. In fact, this coexistence can arise in NVO only due to the symmetric exchange anisotropies.

DOI: 10.1103/PhysRevB.73.184433 PACS number(s): 75.25.+z, 75.10.Jm, 75.40.Gb

I. INTRODUCTION

Recent studies have identified a family of multiferroics which display a phase transition in which there simultaneously develops long-range incommensurate magnetic and uniform ferroelectric order. Perhaps the most detailed studies have been carried out on the systems[1–4] $Ni_3V_2O_8$ (NVO) and $TbMnO_3$ (TMO).[5,6] (For a review, see Ref. 7.) This phenomenon has been explained[3] on the basis of a phenomenological model which invokes a Landau expansion in terms of the order parameters describing the incommensurate magnetic order and the order parameter describing the uniform spontaneous polarization. The Landau expansion suggests that a microscopic model would have to involve a trilinear interaction Hamiltonian coupling two spins on adjacent sites and the displacement derivative of their exchange coupling. In the present paper we complement these earlier studies in two major directions. First, we present a detailed combined neutron scattering study and first-principles calculations of the optical phonons of NVO, and thereby identify those having the right symmetry to induce a ferroelectric dipole moment. Second, we expand the exchange tensor to first order in the generalized displacement coordinates, in order to determine which of these displacements are relevant and which corresponding elements of the exchange tensor can generate the observed dipole moment.

On general grounds, one might expect the Dzyaloshinskii-Moriya[8,9] (DM) interaction to play an important role in coupling the spins with a ferroelectric moment.[10] The DM interaction could also generate incommensurate magnetic ordering. However, the situation in NVO turns out to be more subtle: the main incommensurate ordering results from competing isotropic nearest- and next-nearest interactions, and the DM terms only generate additional small transverse magnetic moments, which are *not* crucial for the ferroelectricity.[2–4] Also, we show below that in NVO the ferroelectric moment can result from the displacement derivatives of many elements of the exchange tensor (and not just from the antisymmetric one of the DM interaction). The methodology of the present paper can be extended in a straightforward way to TMO, for instance.

Briefly this paper is organized as follows. In Sec. II we review the earlier work on symmetries of the lattice and of the magnetic structures,[2,4] which are needed for our present calculation. In Sec. III we discuss the first-principles calculations of the zone-center phonons and identify those phonons which transform such as a vector and which are thus candidates to produce a spontaneous polarization. In this section we also present the neutron scattering measurements of the phonon density of states (DOS), which is found to be in good agreement with the calculated spectrum. In Sec. IV we then use the symmetry operations of the crystal to show how the phonon derivatives of the various exchange tensors in the unit cell are related to one another. Then in Sec. V we show that a mean-field treatment of this spin-phonon coupling leads to the results obtained previously[2,4] in a phenomenological model. Here we give expressions for the spontaneous polarization in terms of gradients of the exchange tensor. It would be nice to have a simple model to illustrate these results. However, our studies of two "toy models" in Sec. VI indicate that (similar to Ref. 10) they do not reproduce some essential features of our complete calculation. Finally, our conclusions are summarized in Sec. VII.

II. SYMMETRIES

Here we give a brief review of the symmetry elements relevant to NVO. Although some of this material appeared earlier, it is needed in order to set the ground for the present

TABLE I. General positions within the primitive unit cell for *Cmca* which describe the symmetry operations of this space group. 2_α is a twofold rotation (or screw) axis and m_α is a mirror (or glide) plane. The primitive translation vectors are $\mathbf{a}_1=(a/2)\hat{i}+(b/2)\hat{j}$, $\mathbf{a}_2=(a/2)\hat{i}-(b/2)\hat{j}$, and $\mathbf{a}_3=c\hat{k}$, where $a=5.92170$ Å, $b=11.37105$ Å, and $c=8.22638$ Å (Refs. 4 and 12).

$E\mathbf{r}=(x,y,z)$	$2_z\mathbf{r}=(\bar{x}+1/2,\bar{y},z+1/2)$
$2_y\mathbf{r}=(\bar{x}+1/2,y,\bar{z}+1/2)$	$2_x\mathbf{r}=(x,\bar{y},\bar{z})$
$\mathcal{I}\mathbf{r}=(\bar{x},\bar{y},\bar{z})$	$m_z\mathbf{r}=\left(x+\frac{1}{2},y,\bar{z}+\frac{1}{2}\right)$
$m_y\mathbf{r}=\left(x+\frac{1}{2},\bar{y},z+1/2\right)$	$m_x\mathbf{r}=(\bar{x},y,z)$

analysis of the coupling between the magnetic and elastic degrees of freedom.

A. Space group

First we review the symmetry of the orthorhombic space group of NVO, Cmca (No. 64 in Ref. 11). The space group operations (apart from primitive translations) are specified in Table I. [Here and below, sites within the unit cell are given as fractions of the sides of the *conventional* unit cell, so that (x,y,z) denotes (xa,yb,zc).] We now describe the sets of crystallographically equivalent sites which the various atoms occupy. (Such a set of crystallographically equivalent sites is called a *Wyckoff orbit*.) In NVO there are six such orbits as shown in Table II. The first two are those of the Ni atoms, the first consisting of the two Ni(1) (a) sites (which we call "cross-tie" sites) and the second consisting of the four Ni(2) (*e*) sites (which we call "spine" sites). The four *V*(*f*) sites comprise the third orbit and the oxygen sites are distributed into two (*f*) orbits, one containing four O(1) atoms, the other containing four O(2) atoms, and a (*g*) orbit containing eight O(3) atoms. (The letters *a*, *e*, *f*, *g* classify the site symmetry according to the convention of Ref. 11. The number of sites in the orbit as listed in Ref. 11 is twice what we give here because here we consider the primitive unit cell rather than the conventional unit cell.) The locations of these sites are specified in the second column of Table II. Note that there are two formula units of NVO per unit cell. The Ni sites form buckled planes which resemble a kagomé lattice and three such adjacent planes are shown in Fig. 1. There one sees that the Ni(2) sites (assigned sublattice numbers 1, 2, 3, and 4) form chains along the *x* direction. The Ni(1) sites (assigned sublattice numbers 5 and 6 and in Fig. 8 they are denoted by *c* and *c'*) occupy inversion symmetric sites with bonds to nearest-neighboring spine sites which form a cross tie. To illustrate the use of Table II we find that the eight operations of Table I acting on (0, 0, 0) generate four copies of each of the two sites which are at (0, 0, 0) and $(1/2,0,1/2)$. Similarly one can generate the eight *g* sites by applying in turn the eight operations of Table I to the site at (x,y,z). (In each case it may be necessary to bring the site back into the original unit cell via a primitive translation vector.)

B. Magnetic structures

We now review briefly the nature of the ordered phases which occur as the temperature *T* is lowered at zero external magnetic field.[1,2,4] At high temperatures the system is paramagnetic. When *T* is lowered through $T_{PH}\approx 9.1$ K, an incommensurate phase appears (called the high-temperature incommensurate or HTI phase) in which the Ni spins on the spine chains are oriented very nearly along the *x* axis with a modulation vector also along $\hat{i}$. (The axes are denoted either **a**, **b**, and **c**, or *x*, *y*, and *z* and corresponding unit vectors are denoted $\hat{i}$, $\hat{j}$, and $\hat{k}$.) As *T* is further lowered through $T_{HL}\approx 6.3$ K, transverse order appears at the same incommensurate wave vector and also order appears on the cross-tie sites, as shown in Fig. 2. We call this phase the low-temperature incommensurate or LTI phase. Within experimental uncertainty, these two ordering transitions are continuous. As *T* is lowered through $T_{LC}\approx 4$ K, a discontinuous transition occurs, into a commensurate antiferromagnetic phase. In this phase antiferromagnetism results from the arrangement of spins within the unit cell in such a way that the magnetic unit cell remains identical to the paramagnetic unit cell.

TABLE II. Wyckoff orbits in NVO. In column 2 we give the Wyckoff position and the fractional coordinates and in column 3 the multiplicity of atoms in the orbits listed in column 1. In column 2 we also give the values of the structural parameters (e.g., *x*, *y*, and *z*) as deduced from diffraction data (Refs. 4 and 12) and the corresponding values we find from the structural minimization are given in parentheses. In column 4 we give the symmetry decomposition of the displacements of atoms in each of the Wyckoff orbits into irreducible representations. Here B_{1u}, B_{2u}, and B_{3u} are the vector representations which transform like *z*, *y*, and *x*, respectively.

Atoms	$(x/a,y/b,z/c)$	Wyckoff	Decomposition
Ni(1)	(0,0,0)	2*a*	$A_u+2B_{1u}+2B_{2u}+B_{3u}$
Ni(2)	$(1/4,y/b,1/4)$	4*e*	$A_u+2B_{1u}+B_{2u}+2B_{3u}$
	$y=0.1298$ (0.1304)		$A_g+2B_{1g}+B_{2g}+2B_{3g}$
V(1)	$(0,y,z)$	4*f*	$A_u+2B_{1u}+2B_{2u}+B_{3u}$
	$y=0.3762$ (0.3762)		$2A_g+2B_{1g}+B_{2g}+2B_{3g}$
	$z=0.1197$ (0.1196)		
O(1)	$(0,y/b,z/c)$	4*f*	$A_u+2B_{1u}+2B_{2u}+B_{3u}$
	$y=0.2481$ (0.2490)		$2A_g+2B_{1g}+B_{2g}+2B_{3g}$
	$z=0.2308$ (0.2301)		
O(2)	$(0,y/b,z/c)$	4*f*	$A_u+2B_{1u}+2B_{2u}+B_{3u}$
	$y=0.0011$ (0.0008)		$2A_g+2B_{1g}+B_{2g}+2B_{3g}$
	$z=0.2444$ (0.2441)		
O(3)	$(x/a,y/b,z/c)$	8*g*	$3A_u+3B_{1u}+3B_{2u}+3B_{3u}$
	$x=0.2656$ (0.2703)		$3A_g+3B_{1g}+3B_{2g}+3B_{3g}$
	$y=0.1192$ (0.1184)		
	$z=0.0002$ (0.0012)		

In Refs. 3, 4, 7, and 13 the application of representation theory to the determination and characterization of magnetic structures is discussed in detail. In Table III we give the character table for the irreducible representations (irreps) for an arbitrary wave vector of the form $(q,0,0)$. Because the irreps are one dimensional, each spin basis function is an eigenvector of the symmetry operator with the listed eigenvalue.

In these references it is shown that the HTI phase is described by a set of five complex amplitudes associated with

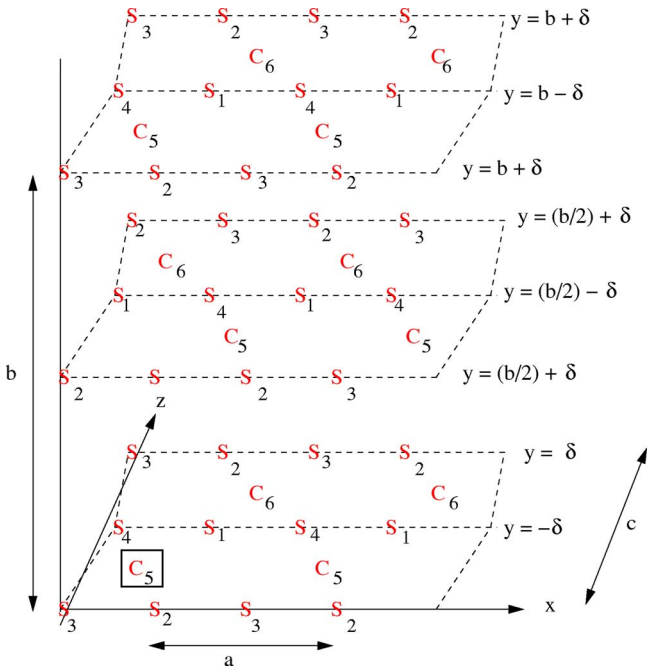

FIG. 1. (Color online) Positions of the Ni(2) spine (S) and Ni(1) cross-tie (C) sites in NVO. The sublattices are numbered as in Eq. (2), below. To make contact with Tables I and II, take the origin to be at the cross-tie site in the box. The buckling is represented by the off set $\delta=0.13b$ of the spine sites. The cross-tie sites have zero off set and are located at $y=0$, $y=b/2$, and $y=b$.

the irrep Γ_4. Here we call these $a_{s,x}$, $ia_{s,y}$, and $a_{s,z}$ to describe the orientation of the spine spins and $a_{c,y}$ and $a_{c,z}$ to describe the orientation of the cross-tie spins. When the LTI phase is entered additional variables associated with the irrep Γ_1 become nonzero. These LTI variables are here denoted $ib_{s,x}$, $b_{s,y}$, and $ib_{s,z}$ to describe the orientation of the spine spins and $b_{c,z}$ to describe the orientation of the cross tie spins. Because the crystal is centrosymmetric, it is shown[4,7,13] that within a given representation all these complex structural parameters (the a's and b's) can be written in terms of a real amplitude times a complex phase factor which is the same for all variables of the same irrep, Γ_4 or Γ_1, in the sense that

$$a_{t,\alpha} = a'_{t,\alpha} e^{i\phi_{HTI}}, \quad b_{t,\alpha} = b'_{t,\alpha} e^{i\phi_{LTI}}, \tag{1}$$

where $a'_{t,\alpha}$ and $b'_{t,\alpha}$ are real (positive or negative), and t denotes either spine or cross tie. It is further expected[4,13] that $\phi_{\mathrm{HTI}} - \phi_{\mathrm{LTI}}$ is $\pm\pi/2$. Thus in these two phases we may use the results of Table VIII in Ref. 4 to write the spin components of the six Ni ions in the unit cell as

$$S_x^{(1)}(\mathbf{R}_1) = (a_{s,x} + ib_{s,x}) e^{i\mathbf{q}\cdot\mathbf{R}_1} + \text{c.c.},$$

$$S_y^{(1)}(\mathbf{R}_1) = (ia_{s,y} + b_{s,y}) e^{i\mathbf{q}\cdot\mathbf{R}_1} + \text{c.c.},$$

$$S_z^{(1)}(\mathbf{R}_1) = (a_{s,z} + ib_{s,z}) e^{i\mathbf{q}\cdot\mathbf{R}_1} + \text{c.c.},$$

$$S_x^{(2)}(\mathbf{R}_2) = (-a_{s,x} + ib_{s,x}) e^{i\mathbf{q}\cdot\mathbf{R}_2} + \text{c.c.},$$

$$S_y^{(2)}(\mathbf{R}_2) = (ia_{s,y} - b_{s,y}) e^{i\mathbf{q}\cdot\mathbf{R}_2} + \text{c.c.},$$

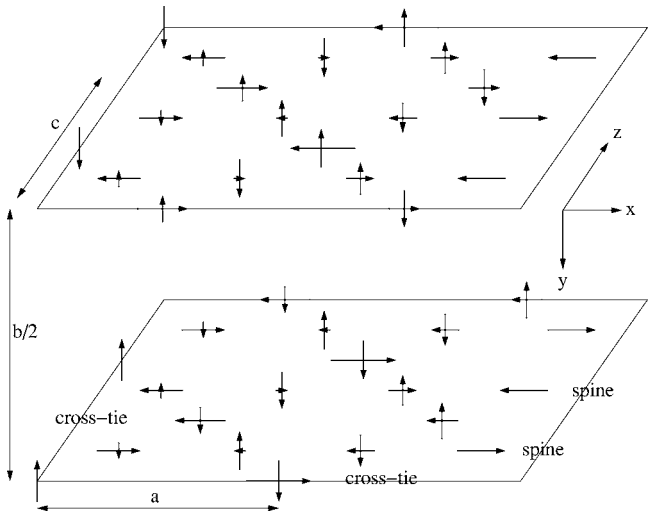

FIG. 2. Schematic diagram showing the x and y components of the spins in the LTI phase. We used the parameters: $q=0.28(2\pi/a)$, $a_{s,x}=1.6$, $a_{c,y}=1.4$, $b_{s,y}=1.3$, $b_{c,x}=-2.2$, and $\phi_{LTI}=\phi_{HTI}+\pi/2$ [see Eq. (1)]. The small z components of spin are not represented. The planes are buckled, so that alternately spine chains are displaced above and below the planes shown (but this buckling is not shown). In the HTI phase the cross-ties have negligible moments and the spine chains have the incommensurately modulated longitudinal moments similar to those shown. The a spin components are odd under 2_x and the b spin components are even under 2_x, where 2_x is a twofold rotation about the x axis. Both spin components (which are pseudovectors) are even under $\tilde{m}_z$.

$$S_z^{(2)}(\mathbf{R}_2) = (a_{s,z} - ib_{s,z}) e^{i\mathbf{q}\cdot\mathbf{R}_2} + \text{c.c.},$$

$$S_x^{(3)}(\mathbf{R}_3) = (a_{s,x} - ib_{s,x}) e^{i\mathbf{q}\cdot\mathbf{R}_3} + \text{c.c.},$$

$$S_y^{(3)}(\mathbf{R}_3) = (-ia_{s,y} + b_{s,y}) e^{i\mathbf{q}\cdot\mathbf{R}_3} + \text{c.c.},$$

$$S_z^{(3)}(\mathbf{R}_3) = (a_{s,z} - ib_{s,z}) e^{i\mathbf{q}\cdot\mathbf{R}_3} + \text{c.c.},$$

$$S_x^{(4)}(\mathbf{R}_4) = (-a_{s,x} - ib_{s,x}) e^{i\mathbf{q}\cdot\mathbf{R}_4} + \text{c.c.},$$

$$S_y^{(4)}(\mathbf{R}_4) = (-ia_{s,y} - b_{s,y}) e^{i\mathbf{q}\cdot\mathbf{R}_4} + \text{c.c.},$$

$$S_z^{(4)}(\mathbf{R}_4) = (a_{s,z} + ib_{s,z}) e^{i\mathbf{q}\cdot\mathbf{R}_4} + \text{c.c.},$$

$$S_x^{(5)}(\mathbf{R}_5) = b_{c,x} e^{i\mathbf{q}\cdot\mathbf{R}_5} + \text{c.c.},$$

TABLE III. Irreducible representations of the group $G_{\mathbf{v}}$ for the incommensurate magnetic structure with $\mathbf{v}=(q,0,0)$. Here it is simplest to use the symmetry operations $\tilde{m}_y$ and $\tilde{m}_z$, such that $\tilde{m}_y\mathbf{r}=(x,\bar{y}+\frac{1}{2},z+\frac{1}{2})$ and $\tilde{m}_z\mathbf{r}=(x,y+\frac{1}{2},\bar{z}+\frac{1}{2})$.

	1	2_x	$\tilde{m}_y$	$\tilde{m}_z$
Γ_1	1	1	1	1
Γ_2	1	1	−1	−1
Γ_3	1	−1	1	−1
Γ_4	1	−1	−1	1

$$S_y^{(5)}(\mathbf{R}_5) = a_{c,y}e^{i\mathbf{q}\cdot\mathbf{R}_5} + \text{c.c.},$$

$$S_z^{(5)}(\mathbf{R}_5) = a_{c,z}e^{i\mathbf{q}\cdot\mathbf{R}_5} + \text{c.c.},$$

$$S_x^{(6)}(\mathbf{R}_6) = -b_{c,x}e^{i\mathbf{q}\cdot\mathbf{R}_6} + \text{c.c.},$$

$$S_y^{(6)}(\mathbf{R}_6) = -a_{c,y}e^{i\mathbf{q}\cdot\mathbf{R}_6} + \text{c.c.},$$

$$S_z^{(6)}(\mathbf{R}_6) = a_{c,z}e^{i\mathbf{q}\cdot\mathbf{R}_6} + \text{c.c.} \quad (2)$$

Here $\mathbf{R}_n$ is the position of a spin n (see Fig. 1). Also $\mathbf{q}=q\hat{i}$ with $q\approx 0.28(2\pi/a)$.[2,4]

As the temperature is varied the magnitudes of these spin components $a_{t,\alpha}$ and $b_{t,\alpha}$ will vary. In contrast, their relative amplitudes are proportional to the components of the appropriate eigenvector of the quadratic free energy matrix and are therefore only weakly temperature dependent. Since the spin variables of a given irrep all have the same complex phase, as in Eq. (1), we write

$$a_{t,\alpha} = \sigma_{\text{HTI}}\tilde{a}_{t,\alpha}, \quad b_{t,\alpha} = \sigma_{\text{LTI}}\tilde{b}_{t,\alpha}, \quad (3)$$

where $\tilde{a}_{t,\alpha}$ and $\tilde{b}_{t,\alpha}$ are real and are normalized by

$$\sum_{t,\alpha}\tilde{a}_{t,\alpha}^2 = \sum_{t,\alpha}\tilde{b}_{t,\alpha}^2 = 1, \quad (4)$$

and where the overall amplitude and phase factor for each irrep are contained in the complex-valued order parameters σ_{HTI} and σ_{LTI}. Thus the order parameters $\sigma_X(\mathbf{q})$ characterize the incommensurate order at wave vector $\mathbf{q}$ of the HTI phase (for $X=H$) and the additional incommensurate order appearing in the LTI phase (for $X=L$).

C. Ferroelectricity

Perhaps surprisingly, it was found that ferroelectricity appears only together with the LTI order, and this behavior was explained by a Landau expansion of the interaction V in powers of order parameters[3]

$$V = \sum_{\alpha}\sum_{X,Y=L,H} a_{\alpha,X,Y}\sigma_X(\mathbf{q})\sigma_Y(-\mathbf{q})P_\alpha, \quad (5)$$

where α labels the Cartesian component of the uniform spontaneous polarization vector $\mathbf{P}$. Using the symmetry properties of the order parameters, $\sigma_H(\mathbf{q})$ and $\sigma_L(\mathbf{q})$, it was shown that only $a_{y,L,H}$ and $a_{y,H,L}$ (which involve *two* different irreps) are nonzero, providing a phenomenological explanation for the experimental finding that a nonzero polarization is induced by incommensurate magnetism only in the LTI phase and then only with $\mathbf{P}$ along the $\mathbf{b}$ axis.

From the form of Eq. (5), it is clear that the spin-phonon Hamiltonian we seek in the present paper must be of the form

$$V_{\text{sp-ph}} = \sum_{i,j,k}\sum_{\alpha\beta\gamma} b_{\alpha\beta\gamma_k}(i,j)S_\alpha(i)S_\beta(j)Q_{\gamma_k}, \quad (6)$$

where $\mathbf{S}(i)$ is the vector spin operator for site i and Q_{γ_k} is the kth normal mode amplitude at zero wave vector which transforms such as the γ component of a first rank tensor (vector). We discuss the normal modes in some detail in the next section. To implement the interaction of Eq. (6) it is convenient to classify both the normal modes and the spin components according to their transformation properties. This interaction represents a linear potential, i.e., a force on the phonon coordinate Q_{γ_k}. Up to quadratic order in the displacements the terms in the elastic potential energy V_{el} which depend on the Q_{γ_k} are

$$V_{\text{el}} = \frac{1}{2}\sum_{\gamma,k}\omega_{\gamma_k}^2 Q_{\gamma_k}^2 + V_{\text{sp-ph}}. \quad (7)$$

Minimization of this elastic energy with respect to the phonon coordinates leads to a phonon displacement which is proportional to the product of two spin functions, whose symmetry we analyze below. Furthermore, since the displaced ions carry an electric charge (albeit an effective charge), these displacements give rise to a spontaneous polarization provided that the necessary spin components are nonzero.

III. ZONE-CENTER PHONONS; NEUTRON SCATTERING MEASUREMENTS AND FIRST PRINCIPLES CALCULATIONS

A. Generalized displacements

Since the normal modes at zero wave vector are complicated linear combinations of atomic displacements, it is useful to introduce symmetry adapted generalized displacements (GD's) which are linear combinations of atomic displacements which transform according to the various irreducible representations as listed in Table II. To discuss ferroelectricity we only need to consider those GD's which transform according to the vector irreps B_{nu}, for $n=1,2,3$ and which therefore transform such as the coordinates z, y, and x, respectively. A GD consists of displacements confined to a single Wyckoff orbit labeled τ and it involves displacements only along a single coordinate axis β because there are no symmetry elements which connect different values of β. Obviously, the use of symmetry is helpful because, as we will see in the next subsection, each normal mode (at zero wave vector) of symmetry B_{nu} consists of a linear combination of the relatively small number of GD's having B_{nu} symmetry.

We start by giving a qualitative discussion of these GD's. Since the irreps are one dimensional, the characters given in Table IV are actually the eigenvalues of the corresponding operations. First of all, one sees that assigning all atoms of a given Wyckoff orbit the *same* displacement along the α axis gives a GD which transforms under the symmetry operations of the space group (given in Table I) such as the α component of a vector. Since NVO has six crystallographically inequivalent sites this construction gives six x-like GD's $x_1, x_2, \ldots, x_6$ in which respectively all Ni(1), Ni(2), V(1), O(1), O(2), or O(3) atoms are displaced equally along the x axis. The analogous y-like GD's are denoted y_n and the analogous z-like GD's are denoted z_n for $n=1,2,\ldots,6$.

We now discuss the construction of the less trivial GD's which have displacements in the β direction but which nev-

TABLE IV. Irreducible representation of the paramagnetic space group of NVO. The vector representations are B_{1u}, B_{2u}, and B_{3u}, which transform like z, y, and x, respectively.

	1	2_y	2_x	2_z	$\mathcal{I}$	m_y	m_x	m_z	Function
A_g	1	1	1	1	1	1	1	1	x^2, y^2, z^2
A_u	1	1	1	1	−1	−1	−1	−1	xyz
B_{2g}	1	1	−1	−1	1	1	−1	−1	xz
B_{2u}	1	1	−1	−1	−1	−1	1	1	y
B_{3g}	1	−1	1	−1	1	−1	1	−1	yz
B_{3u}	1	−1	1	−1	−1	1	−1	1	x
B_{1g}	1	−1	−1	1	1	−1	−1	1	xy
B_{1u}	1	−1	−1	1	−1	1	1	−1	z

ertheless transform like the coordinate α. To generate these GD's, one can start with an arbitrarily chosen site to which a vector displacement along one of the three coordinate axes is specified. Then one generates the displacements of the other sites in the Wyckoff orbit so as to reproduce the desired transformation properties. For example, to construct a z-like mode on the spines, we could assign the lower left spine site (in the lower left panel of Fig. 3) a displacement along the x axis. To be a z-like mode the pattern of displacements should be even under m_x, which fixes the displacement of the lower right spine to be that shown. Such a z-like mode should be odd under a twofold rotation about an x axis passing through the center of the cell. Applying this operation to the two lower spine sites fixes the orientation of the displacements of the upper spine sites. The other four symmetry operations give these same displacements.

Had we started with a spine site with a displacement along the y axis, we would have gotten a null displacement because this symmetry with displacements along the y axis is not allowed. Had we fixed the first site to have a displacement along the z axis we would have found the trivial GD in which all spin sites are displaced in parallel. The other GD's shown in the figures were generated in the same way. It is easy to see that these modes couple to the uniform displacements. For instance, consider the mode z_8 shown in Fig. 3 and in particular consider how the ionic displacements of the spine sites which are shown affect the cross-tie sites (not shown) at the corners and center of the square. Imagine the ion-ion interactions to be repulsive. Then the nearest neighbors at negative z relative to each cross tie get closer to the cross tie and the nearest neighbors at positive z relative to each cross tie get farther away from the cross tie. Thus, all cross ties are squeezed towards positive z in a uniform z mode. This same reasoning also shows that even though this motion is confined to the x direction, it induces a dipole moment along the z direction. Of course, the actual normal modes (phonons) consist of linear combinations of GD's having the same irrep label and they are discussed in the next section.

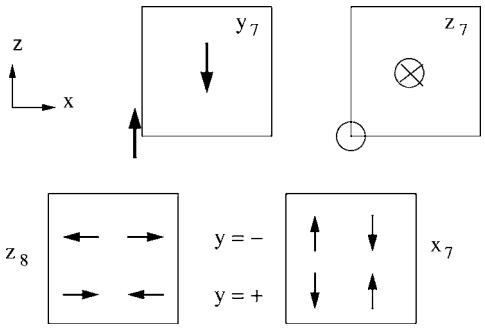

FIG. 3. Generalized displacements y_7, z_7, z_8, and x_7 which transform like the components of a vector, for cross-tie sites (upper panels) and spine sites (lower panels). Atomic displacements (for the GD's indicated by the labels) in the x-z plane are represented by arrows, whereas those in the $+y$ direction ($-y$ direction) are indicated by crossed (open) circles.

B. Normal modes

In this section we present inelastic neutron scattering (INS) measurements of the phonon density of states (DOS) in NVO, and then we compare these results with the first-principles calculations of the zone-center phonons. We identify the phonons which have the correct symmetry to induce a spontaneous polarization, and then we attempt to identify and estimate the local distortion which gives rise to the observed dipole moment in NVO.

The INS measurements were performed using the filter analyzer spectrometer (FANS) located on beamline BT4 at the NIST Center for Neutron Research.[14] For energies above 40 meV, a Cu(220) monochromator, surrounded by $60'-40'$ horizontal collimation and combined with a cooled polycrystalline beryllium filter analyzer was used. For the low energy spectrum (i.e., $E<40$ meV), a graphite (PG) monochromator with $20'-20'$ collimation was used. The relative energy resolution of the FANS instrument is approximately 5% in the energy range probed. The powder $Ni_3V_2O_8$ sample (about 20 grams) was held at 12 K (paramagnetic phase) and 8 K (HTI phase) with a helium-filled aluminum can using a closed-cycle He^3 refrigerator.

The first-principles total-energy and phonon calculations were performed by the plane-wave implementation of the spin-polarized generalized gradient approximation (SP-GGA) to density functional theory (DFT).[15] We used $4\times4\times3$ k points according to Monkhorst-pack scheme and Vanderbilt ultrasoft pseudopotentials for which a cutoff energy of 400 eV was found to be enough for total energies to

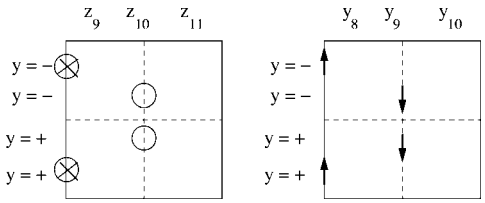

FIG. 4. As Fig. 3. Here we illustrate schematically the vector GD's z_9, z_{10}, z_{11}, y_8, y_9, and y_{10} for f sites. The placement of the sites reproduces the symmetry of an f site and is not quantitative for either V or O atoms. Three distinct f sites are occupied, one by a V atom and the other two by O atoms.

converge within 0.5 eV/atom. We considered the primitive unit cell of the NVO which contains 26 atoms as listed in Table II. Experimental lattice parameters were used in the calculations but the atomic positions were optimized to eliminate the forces down to 0.02 eV/Å. The optimized positions are listed in Table II, showing excellent agreement with the experimental positions. Using the optimized structure, we next calculated the zone-center phonons and the corresponding INS one-phonon spectrum as described in Ref. 16.

The measured INS spectrum along with the calculation are shown in Fig. 6. Since we observed almost identical spectra in the paramagnetic (T=12 K) and the HTI (T =8 K) phases, we show only the sum of these two spectra, in order to gain statistics. The agreement of the calculations to the observed spectrum is quite good, giving further confidence that the first-principle calculations capture the main physics. It also suggests that the phonon modes in NVO have small dispersion with wave vector. This is because the INS spectrum is approximately averaged over a large range of wave vectors and the calculations are only for zero wave vector. The biggest difference between the INS spectrum and the calculation is for the observed feature near 80 meV, which is calculated to be around 70 meV. As we discuss in detail below, interestingly this phonon has the right symmetry and the atomic displacement vector to induce a large dipole moment. Hence, maybe the disagreement for the energy of this mode could be some indication of strong spin-phonon coupling.

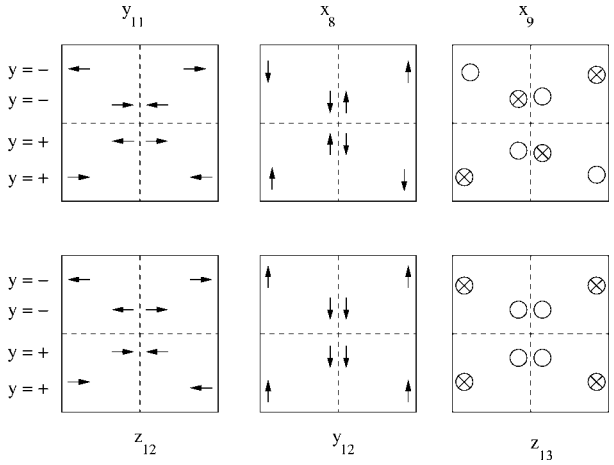

FIG. 5. As Fig. 4. Here we illustrate schematically the vector GD's y_{11}, x_8, x_9, z_{12}, y_{12}, and z_{13} for g sites.

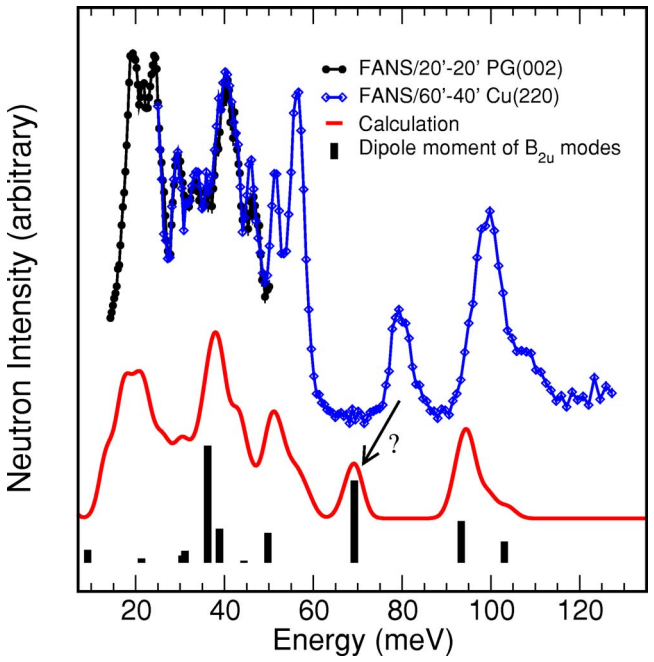

FIG. 6. (Color online) The observed and calculated INS spectrum. The black vertical bars show the B_{2u} phonons whose intensity is proportional to the induced dipole moment when the system is distorted by the zero-point rms values of the modes.

In order to identify those phonon modes that can induce the observed dipole moment along the **b** axis in NVO, we carried out the symmetry analysis of the zone center phonons. Table IV shows the character table for the irreducible representations (irreps) of the group $G_{\mathbf{v}}$ for optical phonons at zero wave vector **v**. (For a review of group theory see Ref. 17.) There are 26 atoms in the primitive unit cell and the representation Γ_u induced by the vector space of these $26\times 3=78$ atomic displacements has the decomposition

$$\Gamma_u = 10A_g + 8A_u + 8B_{1g} + 13B_{1u} + 7B_{2g} + 12B_{2u} + 11B_{3g} + 9B_{3u}. \quad (8)$$

One can check that the vector representations which transform like x, y, and z are B_{3u}, B_{2u}, and B_{1u}, respectively. To discuss the spontaneous polarization these are the only irreps we need to consider. Among the 78 phonons, twelve have B_{2u} symmetry, and can therefore produce the observed[3] spontaneous polarization along the **b** axis. One of the these twelve modes is acoustic (i.e., all atoms move uniformly along the **b** axis) and will not be considered any further. To calculate the phonon energies and wavefunctions we found the eigenvalues ω_n^2 of the matrix **W**, which is related to zero wave vector Fourier transform of the potential energy matrix by $W_{\tau,\alpha;\tau',\alpha'}=M_\tau^{-1/2}V_{\tau,\alpha;\tau',\alpha'}M_{\tau'}^{-1/2}$, where τ labels sites within the primitive unit cell, α labels Cartesian components, and M_τ is the mass of the atom at site τ. The energies ω of the eleven y-like optical modes are shown in Fig. 6 by black bars whose height for mode n is proportional to the y component of the average polarization $\mathbf{P}^{(n)}_{\mathrm{rms},y}$, given by Eq. (10) below.

TABLE V. Mass-weighted atomic displacements $O^{(n)}_{\tau,\alpha}$ of B_{2u} phonons which induce a dipole moment along the **b** axis (normalized so that the sum over all 26 atoms in the unit cell of the squares of the components equals unity for each mode). (The acoustic B_{2u} phonon is not tabulated.) Each component of the mass-weighted displacement represents the atomic displacement times the square root of the respective atomic mass. The mass-weighted displacements are given for the sites listed in column 2 of Table II. The displacements of the remaining atoms in each Wyckoff orbit are fixed so that the mode transforms like B_{2u}, i.e., such as the y component of a vector, (Ref. 18), see Figs. 3–5. The calculated atomic charges $q \equiv q_\tau$, magnitude of the rms displacement $Q_{\mathrm{rms}}/\sqrt{m_p}$ (where m_p is the proton mass), the rms dipole moment along the **b** axis, P_{rms}, and the mode energy ω are also given.

	Ni(1) $q=0.90e$ $(0,y,z)$		Ni(2) $q=0.86e$ $(0,y,0)$	V(1) $q=1.18e$ $(0,y,z)$		O(1) $q=-0.62e$ $(0,y,z)$		O(2) $q=-0.68e$ $(0,y,z)$		O(3) $q=-0.59e$ (x,y,z)			ω	$\frac{Q_{\mathrm{rms}}}{\sqrt{m_p}}$	P_{rms}
Mode	y	z	y	y	z	y	z	y	z	x	y	z	(meV)	(Å)	(10^{-4} C/m^2)
4	0.023	−0.446	−0.119	0.040	0.169	−0.032	−0.015	0.025	−0.314	−0.024	0.005	0.048	9.2	0.47	2.5
16	0.551	−0.007	−0.209	−0.094	−0.063	−0.099	−0.111	−0.061	0.069	0.013	0.073	−0.001	21.3	0.31	1.7
27	−0.205	0.058	−0.110	0.206	0.172	−0.006	−0.354	0.023	−0.061	0.071	0.041	0.009	30.4	0.26	3.3
29	−0.008	−0.428	0.019	0.010	−0.265	0.090	0.050	−0.053	0.086	−0.020	−0.040	−0.178	31.1	0.26	6.1
34	−0.164	0.066	−0.286	0.073	0.049	0.109	0.163	0.103	0.077	−0.073	0.188	−0.068	36.2	0.24	66.1
40	0.178	0.113	−0.166	0.162	−0.012	0.157	0.076	0.171	−0.012	0.029	−0.237	0.007	38.9	0.23	18.7
49	0.069	0.307	0.021	−0.056	−0.138	0.023	0.057	−0.069	−0.348	−0.068	0.015	−0.139	44.4	0.22	0.5
53	−0.014	−0.022	−0.037	−0.043	0.165	0.143	0.182	−0.112	−0.080	0.212	0.066	0.155	49.8	0.20	16.3
64	0.037	0.041	−0.030	0.264	0.110	0.015	0.047	−0.396	0.042	−0.038	−0.027	−0.010	69.2	0.17	46.1
70	0.011	−0.011	0.001	−0.155	0.017	0.365	−0.169	−0.081	0.011	−0.143	−0.004	0.090	93.3	0.15	23.0
78	0.010	0.019	0.004	−0.089	0.238	0.150	−0.099	−0.029	0.000	0.203	0.009	−0.187	103.0	0.14	11.3

The corresponding eigenvectors $O^{(n)}_{\tau,\alpha}$ are given in Table V. Table V also gives the calculated values of the effective charge for the atom at site τ, q_τ (which is calculated by projection of the plane-wave states on localized atomic orbitals by means of Mulliken analysis,[19]), and—for each mode ω—it also lists crude estimates for the average zero-point fluctuation, $Q_{\mathrm{rms}}/\sqrt{m_p} = \sqrt{\hbar/2\omega m_p}$ (this estimate corresponds to the ansatz that the displacement responsible for the spontaneous polarization is equal to the rms zero point displacement) and for the corresponding polarization, $P_{\mathrm{rms},y}$.

As we can see from Fig. 6, half of the B_{2u} modes induce relatively small dipole moments. This is due to the fact that for these phonons, atoms mainly oscillate along the **c** axis and the **b** component of the motion is only a second order effect. However for the other half, the motion is directly along the **b** axis and therefore the induced dipole moment is significant. Animations of these modes and more information can be obtained at Ref. 20. We note that two particular phonons, one at 36 meV and the other around 70 meV, induce a significantly large dipole moment.

To estimate the polarization vector of the nth mode, we write the atomic displacement in terms of the eigenvectors $O^{(n)}_{\tau,\alpha}$ as

$$u_{\tau,\alpha}(\mathbf{R}) = \sum_n O^{(n)}_{\tau,\alpha} M_\tau^{-1/2} Q_n. \tag{9}$$

A crude estimate for the polarization vector of the nth mode (justified only on dimensional grounds) can then be obtained from the following formula:

$$P^{(n)}_{\mathrm{rms},\alpha} = \frac{1}{\Omega_{\mathrm{uc}}} \sum_\tau q_\tau O^{(n)}_{\tau,\alpha} Q_{\mathrm{rms}} M_\tau^{-1/2}, \tag{10}$$

where Ω_{uc} is the volume of the unit cell.

The magnitude of the experimentally observed dipole moment is about $P_{\mathrm{exp}} = 1.25 \times 10^{-4}$ C/m^2. We note that this induced dipole moment is much smaller than the calculated rms dipole moment ($P_{\mathrm{rms}} \sim 46-70 \times 10^{-4}$ C/m^2) listed in Table V. This indicates that the local displacement of the τth atom in the unit cell should be of order $P_{\mathrm{exp}}/P_{\mathrm{rms}} \approx 1/40$ times the rms displacement $Q_{\mathrm{rms}} M_\tau^{-1/2} O^{(n)}_{\tau\alpha}$. For the O(2) atom in mode #64 this would yield a displacement of about 5×10^{-4} Å. This is quite a small distortion and would be very difficult to observe directly by neutron powder diffraction.

Figure 7 shows schematically how the oxygen atoms move in these two particularly interesting phonons. For the low-energy mode 34 at 36 meV, the two oxygen atoms connecting the spine-spins move in the same direction. Therefore, while one of the Ni-O-Ni bond angle decreases, the other Ni-O-Ni bond angle increases. Hence at first order, we do not expect large changes in the Ni-O-Ni superexchange due to this phonon. On the other hand, for the $E=70$ meV mode 64, only one oxygen (which is connected to the cross-tie Ni spin) moves along the **b** axis. Hence, in this case, only one of the Ni-O-Ni bond angles changes from nearly 90° and therefore we expect this phonon to have important effects on the Ni-O-Ni superexchange interaction. Interestingly, the biggest disagreement between the experimental data and the calculated phonon energies happens for this phonon, which further suggests that it may have strong spin-phonon coupling.

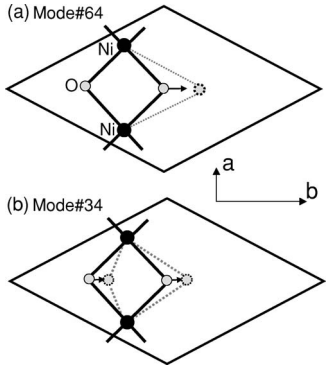

FIG. 7. A schematic representation of the top view of two particularly interesting B_{2u} modes whose displacement vectors are given in Table V. The figure shows the two oxygen and two Ni atoms on *ab* plane ($z \sim 0.25$). The oxygen on the left is connected to V atom. The oxygen on the right is connected to cross-tie Ni which is below the oxygen atom.

IV. RELATIONS FOR THE STRAIN DERIVATIVE OF THE EXCHANGE TENSOR

In this section we obtain explicit forms for the most important spin-phonon coupling matrices. For this purpose we start by introducing notation for the principal exchange interactions. We write the interactions between spins on sites i and j as

$$\mathcal{H}(i,j) = \sum_{\alpha\beta} X_{\alpha\beta}(i,j) S_\alpha(i) S_\beta(j), \tag{11}$$

where $X_{\alpha\beta}(i,j) = X_{\beta\alpha}(j,i)$, of course. For nearest neighbor (NN) interactions between spine spins we set $X_{\alpha\beta}(i,j) = U_{\alpha\beta}(i,j)$, for next nearest neighbor (NNN) interactions between spine spins we set $X_{\alpha\beta}(i,j) = V_{\alpha\beta}(i,j)$, and for NN interactions between spine and cross-tie spins we set $X_{\alpha\beta}(i,j) = W_{\alpha\beta}(i,j)$. We may further decompose the exchange tensor into its symmetric and antisymmetric parts. For example, for NN spine-spine interactions we write (omitting the site labels i and j)

$$\mathbf{U} = \begin{bmatrix} J_{xx} & J_{xy} + D_z & J_{xz} - D_y \\ J_{xy} - D_z & J_{yy} & J_{yz} + D_x \\ J_{xz} + D_y & J_{yz} - D_x & J_{zz} \end{bmatrix}, \tag{12}$$

where $\mathbf{D}$ is the Dzyaloshinskii-Moriya (DM) vector.[8,9] Similar decompositions will be made for $\mathbf{V}$ and $\mathbf{W}$ in terms of symmetric tensors $\mathbf{K}$ and $\mathbf{L}$, respectively, and the DM vectors $\mathbf{E}$ and $\mathbf{F}$, respectively.

Now we consider the gradient expansion of these exchange tensors. For this purpose it is necessary to keep track of the symmetry of the modes, so instead of the mode index n, we assign each mode a symmetry label γ_k, where γ is a symmetry label (whose only values of interest to us are x, y, and z) and the numerical index k distinguishes different modes of the same symmetry. Thus, we rewrite Eq. (9) as

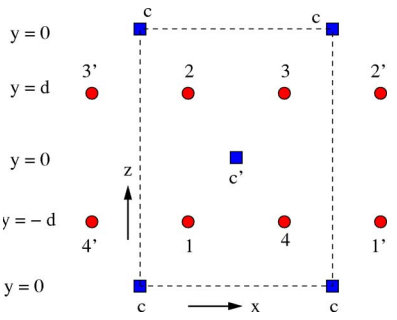

FIG. 8. (Color online) Diagram of an **a**-**c** plane used to specify nearest-neighbor and next-nearest-neighbor interactions along a single spine. Circles are spine sites and square are cross-tie sites and $d = 0.13b$ (see Table II). The dashed rectangle indicates the unit cell. Interactions in other **a**-**c** planes are obtained by using translation symmetry.

$$u_{\tau,\alpha}(\mathbf{R}) = \sum_{\gamma k} O_{\tau,\alpha}^{(\gamma_k)} M_\tau^{-1/2} Q_{\gamma_k}. \tag{13}$$

Then if Z represents a component of an exchange tensor, we write

$$\frac{\partial Z}{\partial Q_{\gamma_k}} = \sum_{\mathbf{R}\tau\alpha} \frac{\partial Z}{\partial u_{\tau,\alpha}(\mathbf{R})} O_{\tau\alpha}^{(\gamma k)} M_\tau^{-1/2}. \tag{14}$$

The aim of the present paper is to determine which such derivatives are required to completely determine the trilinear spin-phonon coupling. The actual calculation of these derivatives is currently in progress. Thus, for normal mode γ_p, we consider the interaction

$$\mathcal{H}_{\gamma_p} = \frac{1}{2} Q_{\gamma_p} \sum_{\alpha\beta} \sum_{ij} \frac{\partial X_{\alpha\beta}(i,j)}{\partial Q_{\gamma_p}} S_\alpha(i) S_\beta(j). \tag{15}$$

Our objective is to express the results for the spontaneous polarization due to the trilinear coupling in terms of the parameters $\partial X_{\alpha\beta}(i,j)/\partial Q_{\gamma_p}$.

Here we analyze the gradients of the NN interactions between spine spins. (Similar analyses of next-nearest neighbor spine interactions and of NN spine-cross tie interactions are given in Appendixes.) We introduce the coupling between spine sites 1 and 4 in Fig. 8

$$\frac{\partial U_{\alpha\beta}(1,4)}{\partial Q_{\gamma_p}} \equiv U_{\alpha\beta}^{\gamma_p}. \tag{16}$$

Clearly $\mathcal{H}_{\gamma_p}$ has to be invariant under the symmetry operations of the crystal. But m_x takes the bond in question into itself (and interchanges indices). This indicates that these interaction matrices must satisfy

$$\boldsymbol{\sigma}_x \mathbf{U}^{x_p} \boldsymbol{\sigma}_x = -\tilde{\mathbf{U}}^{x_p},$$

$$\boldsymbol{\sigma}_x \mathbf{U}^{y_p} \boldsymbol{\sigma}_x = \tilde{\mathbf{U}}^{y_p},$$

$$\boldsymbol{\sigma}_x \mathbf{U}^{z_p} \boldsymbol{\sigma}_x = \tilde{\mathbf{U}}^{z_p}, \tag{17}$$

where tilde indicates transpose

$$\boldsymbol{\sigma}_x = \begin{bmatrix} -1 & 0 & 0 \\ 0 & 1 & 0 \\ 0 & 0 & 1 \end{bmatrix},$$

and later

$$\boldsymbol{\sigma}_y = \begin{bmatrix} 1 & 0 & 0 \\ 0 & -1 & 0 \\ 0 & 0 & 1 \end{bmatrix},$$

$$\boldsymbol{\sigma}_z = \begin{bmatrix} 1 & 0 & 0 \\ 0 & 1 & 0 \\ 0 & 0 & -1 \end{bmatrix}. \tag{18}$$

Here we used the fact that the normal modes have a known symmetry

$$m_\alpha Q_{\beta_p} = (1 - 2\delta_{\alpha,\beta}) Q_{\beta_p}, \tag{19}$$

and

$$2_\alpha Q_{\beta_p} = (-1 + 2\delta_{\alpha,\beta}) Q_{\beta_p}. \tag{20}$$

In view of Eq. (17), we have

$$\mathbf{U}^{x_p} = \begin{bmatrix} 0 & J^x_{xy} & J^x_{xz} \\ J^x_{xy} & 0 & D^x_x \\ J^x_{xz} & -D^x_x & 0 \end{bmatrix},$$

$$\mathbf{U}^{y_p} = \begin{bmatrix} J^y_{xx} & D^y_z & -D^y_y \\ -D^y_z & J^y_{yy} & J^y_{yz} \\ D^y_y & J^y_{yz} & J^y_{zz} \end{bmatrix},$$

$$\mathbf{U}^{z_p} = \begin{bmatrix} J^z_{xx} & D^z_z & -D^z_y \\ -D^z_z & J^z_{yy} & J^z_{yz} \\ D^z_y & J^z_{yz} & J^z_{zz} \end{bmatrix}, \tag{21}$$

where the index p on the superscripts of J and D are left implicit and $J^{\gamma_p}_{\alpha\beta}$ and $D^{\gamma_p}_\alpha$ (and similarly later for superscripts on $\mathbf{K}$, $\mathbf{L}$, $\mathbf{E}$, and $\mathbf{F}$) are defined to be

$$J^{\gamma_p}_{\alpha\beta} \equiv \frac{\partial J_{\alpha\beta}(1,4)}{\partial Q_{\gamma_p}}, \quad D^{\gamma_p}_\alpha \equiv \frac{\partial D_\alpha(1,4)}{\partial Q_{\gamma_p}}. \tag{22}$$

Then we obtain the 2-3 interaction from the above by 2_x, a twofold rotation about the x axis, so that

$$\frac{\partial U_{\alpha\beta}(2,3)}{\partial Q_{x_p}} = \boldsymbol{\sigma}_y \boldsymbol{\sigma}_z \mathbf{U}^{x_p} \boldsymbol{\sigma}_y \boldsymbol{\sigma}_z = \begin{bmatrix} 0 & -J^x_{xy} & -J^x_{xz} \\ -J^x_{xy} & 0 & D^x_x \\ -J^x_{xz} & -D^x_x & 0 \end{bmatrix}, \tag{23}$$

$$\frac{\partial U_{\alpha\beta}(2,3)}{\partial Q_{y_p}} = -\boldsymbol{\sigma}_y \boldsymbol{\sigma}_z \mathbf{U}^{y_p} \boldsymbol{\sigma}_y \boldsymbol{\sigma}_z = \begin{bmatrix} -J^y_{xx} & D^y_z & -D^y_y \\ -D^y_z & -J^y_{yy} & -J^y_{yz} \\ D^y_y & -J^y_{yz} & -J^y_{zz} \end{bmatrix}, \tag{24}$$

$$\frac{\partial U_{\alpha\beta}(2,3)}{\partial Q_{z_p}} = -\boldsymbol{\sigma}_y \boldsymbol{\sigma}_z \mathbf{U}^{z_p} \boldsymbol{\sigma}_y \boldsymbol{\sigma}_z = \begin{bmatrix} -J^z_{xx} & D^z_z & -D^z_y \\ -D^z_z & -J^z_{yy} & -J^z_{yz} \\ D^z_y & -J^z_{yz} & -J_{zz} \end{bmatrix}, \tag{25}$$

where we used Eq. (20).

We obtain the 4-1′ interactions by applying the glide operation m_y to the 2-3 interaction, so that

$$\frac{\partial U_{\alpha\beta}(4,1')}{\partial Q_{x_p}} = \boldsymbol{\sigma}_y \frac{\partial \mathbf{U}(2,3)}{\partial Q_{x_p}} \boldsymbol{\sigma}_y = \begin{bmatrix} 0 & J^x_{xy} & -J^x_{xz} \\ J^x_{xy} & 0 & -D^x_x \\ -J^x_{xz} & D^x_x & 0 \end{bmatrix}, \tag{26}$$

$$\frac{\partial U_{\alpha\beta}(4,1')}{\partial Q_{y_p}} = -\boldsymbol{\sigma}_y \frac{\partial \mathbf{U}(2,3)}{\partial Q_{y_p}} \boldsymbol{\sigma}_y = \begin{bmatrix} J^y_{xx} & D^y_z & D^y_y \\ -D^y_z & J^y_{yy} & -J^y_{yz} \\ -D^y_y & -J^y_{yz} & J^y_{zz} \end{bmatrix}, \tag{27}$$

$$\frac{\partial U_{\alpha\beta}(4,1')}{\partial Q_{z_p}} = \boldsymbol{\sigma}_y \frac{\partial \mathbf{U}(2,3)}{\partial Q_{z_p}} \boldsymbol{\sigma}_y = \begin{bmatrix} -J^z_{xx} & -D^z_z & -D^z_y \\ D^z_z & -J^z_{yy} & J^z_{yz} \\ D^z_y & J^z_{yz} & -J^z_{zz} \end{bmatrix}, \tag{28}$$

and finally we get the 3-2′ interaction by applying a two-fold rotation about the x axis to the 4-1′ interaction to get

$$\frac{\partial U_{\alpha\beta}(3,2')}{\partial Q_{x_p}} = \boldsymbol{\sigma}_y \boldsymbol{\sigma}_z \frac{\partial \mathbf{U}(4,1')}{\partial Q_{x_p}} \boldsymbol{\sigma}_y \boldsymbol{\sigma}_z = \begin{bmatrix} 0 & -J^x_{xy} & J^x_{xz} \\ -J^x_{xy} & 0 & -D^x_x \\ J^x_{xz} & D^x_x & 0 \end{bmatrix}, \tag{29}$$

$$\frac{\partial U_{\alpha\beta}(3,2')}{\partial Q_{y_p}} = -\boldsymbol{\sigma}_y \boldsymbol{\sigma}_z \frac{\partial \mathbf{U}(4,1')}{\partial Q_{y_p}} \boldsymbol{\sigma}_y \boldsymbol{\sigma}_z = \begin{bmatrix} -J^y_{xx} & D^y_z & D^y_y \\ -D^y_z & -J^y_{yy} & J^y_{yz} \\ -D^y_y & J^y_{yz} & -J^y_{zz} \end{bmatrix}, \tag{30}$$

and

$$\frac{\partial U_{\alpha\beta}(3,2')}{\partial Q_{z_p}} = -\boldsymbol{\sigma}_y \boldsymbol{\sigma}_z \frac{\partial \mathbf{U}(4,1')}{\partial Q_{z_p}} \boldsymbol{\sigma}_y \boldsymbol{\sigma}_z = \begin{bmatrix} J^z_{xx} & -D^z_z & -D^z_y \\ D^z_z & J^z_{yy} & -J^z_{yz} \\ D^z_y & -J^z_{yz} & J^z_{zz} \end{bmatrix}. \tag{31}$$

V. MEAN FIELD SPIN-PHONON HAMILTONIAN

A. Mean field results

Here we treat the NN spine-spine interactions in detail. Analogous calculations for the NNN spine-spine and NN spine-cross tie interactions are treated in Appendix B. We evaluate the spin-phonon Hamiltonian $\mathcal{H}_{\gamma_p}$ of Eq. (15) at the mean-field level. In other words, for the spin operators we

simply substitute their average values as given in Eq. (2). One sees that $\mathcal{H}_{x_p}$ for NN spine-spine interactions, for instance, consists of contributions proportional to $J^{x_p}_{xy}$, to $J^{x_p}_{xz}$, and to $D^{x_p}_{x}$. To illustrate the calculation we explicitly evaluate the first of these, which we denote $\mathcal{H}_{x_p}(J_{xy})$

$$\begin{aligned}\mathcal{H}_{x_p}(J_{xy}) = Q_{x_p} J^{x_p}_{xy} \sum_{uc} [&S_x(1)S_y(4) + S_y(1)S_x(4) - S_x(2)S_y(3) \\ &- S_x(3)S_y(2) + S_x(4)S_y(1') + S_x(1')S_y(4) \\ &- S_x(3)S_y(2') - S_x(2')S_y(3)],\end{aligned} \tag{32}$$

where, since we included all interactions within a single unit cell, the sum is over all $N_{\rm uc}$ unit cells. (In this summation only terms involving both $\mathbf{q}$ and $-\mathbf{q}$ survive.) Thus

$$\begin{aligned}\mathcal{H}_{x_p}(J_{xy}) &= 2N_{\rm uc} Q_{x_p} J^{x_p}_{xy} e^{-iqa/2} [(a_{s,x} + ib_{s,x})(ia^*_{s,y} - b^*_{s,y}) + (ia_{s,y} \\ &\quad + b_{s,y})(-a^*_{s,x} + ib^*_{s,x}) - (-a_{s,x} + ib_{s,x})(ia^*_{s,y} + b^*_{s,y}) \\ &\quad - (ia_{s,y} - b_{s,y})(a^*_{s,x} + ib^*_{s,x})] + \text{c.c.} \\ &= 16N_{\rm uc} Q_{x_p} J^{x_p}_{xy} \cos(qa/2) \Im[a^*_{s,x} a_{s,y} + b_{s,x} b^*_{s,y}].\end{aligned} \tag{33}$$

The other terms proportional to Q_{x_p} are

$$\mathcal{H}_{x_p}(J_{xz}) = 16N_{\rm uc} Q_{x_p} J^{x_p}_{xz} \sin(qa/2) \Im[a_{s,x} a^*_{s,z} + b_{s,x} b^*_{s,z}], \tag{34}$$

$$\mathcal{H}_{x_p}(D_x) = 16N_{\rm uc} Q_{x_p} D^{x_p}_{x} \cos(qa/2) \Im[-a_{s,y} a^*_{s,z} + b_{s,y} b^*_{s,z}]. \tag{35}$$

In view of Eq. (1) all these terms involving Q_{x_p} vanish, as was found from the phenomenological formulation. Similarly, all the terms involving Q_{z_p} also vanish, again in conformity with the phenomenological argument.

We are thus only left with terms involving Q_{y_p}. In Appendix B we find that the strain dependence of the NN spine interactions give

$$\mathcal{H}_{y_p} = 16N_{uc} Q_{y_p} \sum_{\mu,\nu=x,y,z} \Lambda^{(\rm NN)}_{\mu\nu} \Im[a^*_{s,\mu} b_{s,\nu}], \tag{36}$$

where

$$\mathbf{\Lambda}^{(\rm NN)} = \begin{bmatrix} J^{y_p}_{xx} c & D^{y_p}_{z} s & D^{y_p}_{y} c \\ -D^{y_p}_{z} s & -J^{y_p}_{yy} c & -J^{y_p}_{yz} s \\ D^{y_p}_{y} c & J^{y_p}_{yz} s & -J^{y_p}_{zz} c \end{bmatrix}, \tag{37}$$

$c \equiv \cos(qa/2)$ and $s \equiv \sin(qa/2)$. Using the results of Appendix B we find that the NNN interactions give a result of the form of Eq. (36) but with

$$\mathbf{\Lambda}^{(\rm NNN)} = \begin{bmatrix} -K^{y_p}_{xx} c' & -E^{y_p}_{z} s' & -K^{y_p}_{xz} c' \\ E^{y_p}_{z} s' & K^{y_p}_{yy} c' & -E^{y_p}_{x} s' \\ -K^{y_p}_{xz} c' & E^{y_p}_{x} s' & -K^{y_p}_{zz} c' \end{bmatrix}, \tag{38}$$

while $c' \equiv \cos(qa)$ and $s' \equiv \sin(qa)$. Using the results of Appendix B we have the results for the spine-cross tie exchange gradients

$$\begin{aligned}V_{y_p} = 16N_{\rm uc} Q_{y_p} \Bigg(&\sum_{\alpha=y,z} \sum_{\beta} \Lambda^{sx}_{\alpha\beta} \Im[a_{c,\alpha} b^*_{s,\beta}] \\ &+ \sum_{\alpha=x} \sum_{\beta} \Lambda^{sx}_{\alpha\beta} \Im[b_{c,\alpha} a^*_{s,\beta}] \Bigg),\end{aligned} \tag{39}$$

where Λ^{sx} is

$$\begin{bmatrix} L^{y_p}_{xx} s'' & [L^{y_p}_{xy} + F^{y_p}_{z}] c'' & [L^{y_p}_{xz} - F^{y_p}_{y}] s'' \\ [L^{y_p}_{xy} - F^{y_p}_{z}] c'' & L^{y_p}_{yy} s'' & [L^{y_p}_{yz} + F^{y_p}_{x}] c'' \\ [L^{y_p}_{xz} + F^{y_p}_{y}] c'' & [L^{y_p}_{yz} - F^{y_p}_{x}] s'' & L^{y_p}_{zz} c'' \end{bmatrix}, \tag{40}$$

where $c'' \equiv \cos(qa/4)$ and $s'' \equiv \sin(qa/4)$. These results agree with the phenomenological model, in that V_{y_p} is only nonzero when both the "*a*" and the "*b*" irreps are simultaneously present and they can not have the same phase (lest $a^* b$ be real).

B. Summary

Here we show how the above results lead to an evaluation of the spontaneous polarization. If we combine the results of Eqs. (36)–(39), we see that the spin-phonon coupling is of the form

$$V_{y_p} = N_{\rm uc} Q_{y_p} \lambda_{y_p}, \quad p = 1, 12, \tag{41}$$

where the coupling constant λ_{y_p} is determined by Eqs. (36)–(39). Since the unperturbed elastic energy is $\mathcal{H}_0 = (N_{\rm uc}/2) \Sigma_n \omega_n^2 Q_n^2$, we see that the trilinear interaction induces the displacements

$$\langle u_{\tau,\alpha}(\mathbf{R}) \rangle = \sum_k O^{(y_k)}_{\tau,\alpha} M^{-1/2}_{\tau} \langle Q_{y_k} \rangle = \sum_k O^{(y_k)}_{\tau,\alpha} M^{-1/2}_{\tau} \lambda_{y_k} \omega^{-2}_{y_k}. \tag{42}$$

Assuming that the polarization is mainly due to the direct effect of atomic motion (and thereby neglecting moments in the y direction induced by atomic motions in the x and z directions), we then have

$$P_y = \frac{1}{\Omega_{\rm uc}} \sum_{\tau,k} q_\tau O^{(y_k)}_{\tau,y} M^{-1/2}_{\tau} \lambda_{y_k} \omega^{-2}_{y_k}. \tag{43}$$

The only ingredients we do not have for this evaluation are the various gradients of the exchange tensors which determine the coupling constants λ_{y_k}.

VI. TOY MODELS

So far, we have shown that the low symmetry of NVO allows several sources for the trilinear coupling between magnetism and ferroelectricity. Since it is usually tempting to try simple models, we consider in this section two toy models. In the first one, we consider a single spine with one Ni per unit cell, but with two oxygen atoms symmetrically placed on either side of the spine. In this version, all atoms lie in a single plane, see the left panel of Fig. 9. In the second model, the size of the unit cell is doubled. In one plaquette the oxygen atoms are both displaced equally perpendicularly to the original atomic plane (in the z direction) and in the

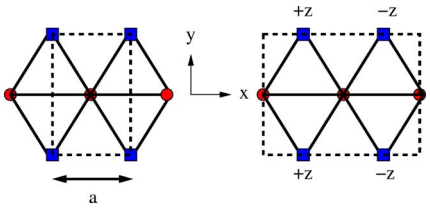

FIG. 9. (Color online) The two toy models. In each case the unit cell is bounded by a dashed line. The filled circles are Ni sites and the squares are O sites.

next plaquette the oxygens are oppositely displaced (see the right panel of Fig. 9). In this version one of the mirror planes becomes a glide plane. These models illustrate the simplifications which arise when the system has higher symmetry than the buckled kagomé lattice of NVO.

A. Unit cell with one Ni atom

In this section we consider the toy model shown in the left panel of Fig. 9. We first analyze the symmetry of the strain derivatives of the exchange tensor. By translational symmetry all nearest neighbor interactions are equivalent. So we set

$$\frac{\partial J_{\alpha\beta}(n,n+1)}{\partial Q_{\gamma_p}} \equiv \mathbf{J}_{\alpha\beta}^{\gamma_p} = \begin{bmatrix} J_{xx}^{\gamma} & J_{xy}^{\gamma}+D_z^{\gamma} & J_{xz}^{\gamma}-D_y^{\gamma} \\ J_{xy}^{\gamma}-D_z^{\gamma} & J_{yy}^{\gamma} & J_{yz}^{\gamma}+D_x^{\gamma} \\ J_{xz}^{\gamma}+D_y^{\gamma} & J_{yz}^{\gamma}-D_x^{\gamma} & J_{zz}^{\gamma} \end{bmatrix}, \tag{44}$$

where $J_{\alpha\beta}^{\gamma} \equiv \partial J_{\alpha\beta}/\partial Q_{\gamma_p}$, $D_{\alpha}^{\gamma} \equiv \partial D_{\alpha}/\partial Q_{\gamma_p}$, and the index p is left implicit. The Hamiltonian is invariant under mirror reflections with respect to each coordinate axis. Taking account of the symmetry of the displacement coordinate and the fact that m_x interchanges indices of the exchange tensor, we have that

$$\begin{aligned} \boldsymbol{\sigma}_x \mathbf{J}^{\gamma} \boldsymbol{\sigma}_x &= (1-2\delta_{x,\gamma})\tilde{\mathbf{J}}^{\gamma}, \\ \boldsymbol{\sigma}_y \mathbf{J}^{\gamma} \boldsymbol{\sigma}_y &= (1-2\delta_{y,\gamma})\mathbf{J}^{\gamma}, \\ \boldsymbol{\sigma}_z \mathbf{J}^{\gamma} \boldsymbol{\sigma}_z &= (1-2\delta_{z,\gamma})\mathbf{J}^{\gamma}. \end{aligned} \tag{45}$$

As a result of this symmetry, all the symmetric exchange derivatives vanish, $J_{\alpha\beta}^{\gamma} \equiv 0$, and the only nonvanishing components of the DM vector derivatives are D_x^y and D_y^z. The resulting trilinear spin-phonon interaction, V, is

$$V = \sum_p \left(Q_{y_p} D_z^{y_p} C_y + Q_{z_p} D_y^{z_p} C_z\right), \tag{46}$$

where

$$C_{\alpha} = \sum_n \left[S_x(n) S_{\alpha}(n+1) - S_{\alpha}(n) S_x(n+1)\right]. \tag{47}$$

Now we replace the spins by their equilibrium values. We note that each spin component belongs to a separate representation and we write

$$\begin{aligned} S_x(n) &= S_x(q) e^{inqa} + S_x(q)^* e^{-inqa}, \\ S_y(n) &= S_y(q) e^{inqa} + S_y(q)^* e^{-inqa}, \\ S_z(n) &= S_z(q) e^{inqa} + S_z(q)^* e^{-inqa}. \end{aligned} \tag{48}$$

Then, keeping only those terms which survive the sum over n we have

$$\begin{aligned} V = 4N \sin(qa) \sum_p \left[Q_{y_p} D_z^{y_p} r_x(q) r_y(q) \sin(\phi_x - \phi_y)\right. \\ \left. + Q_{z_p} D_y^{z_p} r_z(q) r_x(q) \sin(\phi_x - \phi_z)\right], \end{aligned} \tag{49}$$

where N is the total number of Ni spins and we set $S_{\alpha}(q) = r_{\alpha}(q) e^{i\phi_{\alpha}}$, where $r_{\alpha}(q)$ is real. As found before[3,4,7] this interaction is only nonzero when (a) two different representations are condensed and (b) the two representation have different phases ϕ. In view of the results of Eqs. (36)–(39), it is clear that the appearance of only strain derivatives of the DM vector is an artifact of the rather high symmetry of this coplanar model.

B. Unit cell with two Ni atoms

Now we consider the noncoplanar toy model shown in the right panel of Fig. 9. The first two symmetry relations of Eq. (45) remain valid, but the third one now results from the glide plane which involves a translation along the chain. If $\mathbf{J}_{-}^{\alpha}$ denotes the strain derivative of the exchange tensor for coupling sites $2n$ and $2n+1$, and $\mathbf{J}_{+}^{\alpha}$ that for sites $2n+1$ and $2n+2$, then we have

$$\mathbf{J}_{\pm}^{x} = \begin{bmatrix} 0 & 0 & \pm J_{xz}^{x} \\ 0 & 0 & 0 \\ \pm J_{xz}^{x} & 0 & 0 \end{bmatrix}, \tag{50}$$

$$\mathbf{J}_{\pm}^{y} = \begin{bmatrix} 0 & D_z^y & 0 \\ -D_z^y & 0 & \pm J_{yz}^{y} \\ 0 & \pm J_{yz}^{y} & 0 \end{bmatrix}, \tag{51}$$

$$\mathbf{J}_{\pm}^{z} = \begin{bmatrix} \pm J_{xx}^{z} & 0 & -D_y^z \\ 0 & \pm J_{yy}^{z} & 0 \\ D_y^z & 0 & \pm J_{zz}^{z} \end{bmatrix}. \tag{52}$$

Here the superscript in J or D indicates a phonon derivative as in Eq. (44). In this case the relevant generalized displacements Q_{γ_k} are those shown in Fig. 10.

Next we characterize the spin structure. There are four irreps for which the basis functions are listed in Table VI. Thus we write for spins 1 ($\mathbf{S}_1$) and 2 ($\mathbf{S}_2$) in the unit cell

$$S_{1,x}(X) = \left[S_x^{(1)}(q) + S_x^{(2)}(q)\right] e^{iqX} + \text{c.c.}, \tag{53}$$

$$S_{1,y}(X) = \left[S_y^{(3)}(q) + S_y^{(4)}(q)\right] e^{iqX} + \text{c.c.}, \tag{54}$$

$$S_{1,z}(X) = \left[S_z^{(1)}(q) + S_z^{(2)}(q)\right] e^{iqX} + \text{c.c.}, \tag{55}$$

$$S_{2,x}(X) = \left[S_x^{(1)}(q) - S_x^{(2)}(q)\right] e^{iqX} + \text{c.c.}, \tag{56}$$

$$S_{2,y}(X) = \left[S_y^{(3)}(q) - S_y^{(4)}(q)\right] e^{iqX} + \text{c.c.}, \tag{57}$$

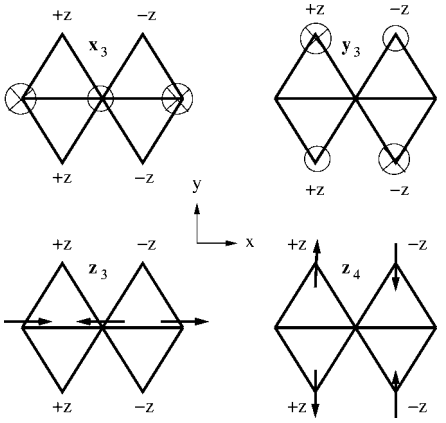

FIG. 10. Generalized displacements which transform like vectors. Open circles (circles with inscribed "*x*") are displacements out of (into) the page. The sites at positive or negative z are indicated. The upper panels show modes in which the atoms move only in the z direction. Upper left: an x-like mode x_3. Upper right: a y-like mode y_3. The lower panels show z-like modes. Left: z_3 with motion only along the x-axis and right: z_4 with motion only along the y axis.

$$S_{2,z}(X) = [-S_z^{(1)}(q) + S_z^{(2)}(q)]e^{iqX} + \text{c.c.}, \tag{58}$$

where the superscript labels the irrep as in Table VI. Thereby we find the trilinear spin-phonon coupling (when the spin operators are replaced by their values)

$$V = 4N\sin(qa)\sum_p \left[UQ_{x_p}J_{xz}^{x_p} + Q_{y_p}(VJ_{yz}^{y_p} + WD_z^{y_p}) + Q_{z_p}\left(XD_y^{z_p} + \sum_{\alpha=x,y,z} Y_\alpha J_{\alpha\alpha}^{z_p}\right)\right], \tag{59}$$

where

$$U = \Im(S_x^{(1)}(q)^* S_z^{(1)}(q) + S_x^{(2)}(q)S_z^{(2)}(q)^*), \tag{60}$$

$$V = \Im(S_y^{(4)}(q)S_z^{(2)}(q)^* + S_z^{(1)}(q)S_y^{(3)}(q)^*), \tag{61}$$

$$W = \Im(S_x^{(1)}(q)S_y^{(3)}(q)^* + S_x^{(2)}(q)^* S_y^{(4)}(q)), \tag{62}$$

$$X = \Im(S_x^{(1)}(q)^* S_z^{(2)}(q) + S_x^{(2)}(q)S_z^{(1)}(q)^*), \tag{63}$$

$$Y_x = \Im(S_x^{(1)}(q)^* S_x^{(2)}(q)), \tag{64}$$

TABLE VI. Basis spin functions for sites #1 and #2 in the unit cell in terms of the complex-valued Fourier components $S_\alpha(q)$ for irreps characterized by the eigenvalues of m_y and the glide operation m_z.

Γ	m_y	m_z	**S**(#1)	**S**(#2)
Γ_1	+	+	$(S_x(q),0,S_z(q))$	$(S_x(q),0,-S_z(q))$
Γ_2	+	−	$(S_x(q),0,S_z(q))$	$(-S_x(q),0,-S_z(q))$
Γ_3	−	+	$(0,S_y(q),0)$	$(0,S_y(q),0)$
Γ_4	−	−	$(0,S_y(q),0)$	$(0,-S_y(q),0)$

$$Y_y = \Im(S_y^{(3)}(q)^* S_y^{(4)}(q)), \tag{65}$$

$$Y_z = \Im(S_z^{(1)}(q)S_z^{(2)}(q)^*). \tag{66}$$

The general symmetry arguments indicate that there cannot be a polarization along $\hat{i}$. We see that U vanishes because all the components within a single representation have the same phase, so that, for instance, $S_x^{(1)}(q)S_z^{(1)}(q)^*$ is real. Here we see that, depending on the spin structure the spontaneous polarization can either be along $\hat{j}$ (if either both irreps 1 and 3 are active or both irreps 2 and 4 are active) or along $\hat{k}$ (if either both irreps 1 and 2 are active or both irreps 3 and 4 are active.) These results are exactly what the phenomenological analysis would give. Thus, one can obtain a spontaneous polarization without invoking gradients of the DM interaction, just as in the full model for NVO.

VII. CONCLUSIONS

In this paper we present neutron scattering measurements of phonons in NVO, the first-principles computation of the zone-center phonons and their symmetry analysis. We identified two particularly interesting phonons among the twelve B_{2u} modes which have the right symmetry to induce the experimentally observed dipole moment along the **b** axis in NVO. Using the calculated atomic charges and the eigenvectors we conclude that the required distortion to induce the observed dipole moment is small (0.001 Å) and would be difficult to observe directly by neutron powder diffraction. Finally, we present a symmetry analysis to characterize the microscopic magnetoelectric coupling in $Ni_3V_2O_8$.

In NVO the spin structure may not be definitively determined. However, according to Ref. 4 one has, in the LTI phase

$$a_{s,x} = 1.6, \quad b_{s,y} = 1.3, \quad a_{c,y} = 1.4, \quad b_{c,x} = -2.2 \tag{67}$$

all in units of Bohr magnetons. Referring to Eqs. (37), (38), and (40), one see that symmetry allows interactions in which the distortion along the **b** axis couples to terms of the type

$$D_z^{y_p}\sin(qa/2)\Im[a_{s,x}^* b_{s,y}],$$

$$L_{yy}^{y_p}\sin(qa/4)\Im[a_{c,y}b_{s,y}^*]. \tag{68}$$

The phonon mechanism in NVO may thus involve the gradient of *either* the DM interaction *or* of the diagonal interaction (which is partly isotropic). If the spin structure is taken for granted, the gradient of the isotropic exchange interaction (namely $L_{yy}^{y_p}$) can produce magnetically induced spontaneous polarization (MISP). This gradient does not involve the spin-orbit interaction. However, to have a spin structure for which $a_{c,y}b_{s,y}^*$ is nonzero undoubtedly requires anisotropic exchange, which *does* require spin-orbit interactions. Contrariwise, one can have MISP due to gradients of the anisotropic interactions (which are nonzero only in the presence of spin-orbit interactions) even when the spin structure results from an isotropic Heisenberg spin Hamiltonian. In any event, the picture of spin-phonon interactions seems

clear: MISP is due to exchange striction, by which one means that exchange energy can be gained at the cost of elastic energy in a suitable static distortion, such that the atomic motion sets up a spontaneous polarization. The method which we used in this paper can easily be applied to similar systems such as $TbMnO_3$.

The result of our analysis is that we can specify those strain derivatives of the exchange tensor which should now be the targets of more fundamental quantum calculations, perhaps based on the LDA[21,22] or similar schemes. In Sec. V B we show how these gradients lead to an evaluation of the spontaneous polarization from first principles. In Sec. VI we also studied some structurally simpler toy models.

A general conclusion is that the local site symmetry in NVO is low enough that almost all strain derivatives of the exchange tensor are involved. However, in contrast to some naive toy models,[10] which require the DM interaction for generating *both* the magnetic incommensurate order *and* the induced ferroelectricity, anisotropic exchange interactions are only needed to either generate a suitable magnetic structure to involve gradients of isotropic exchange interactions or to involve gradients of anisotropic exchange interactions in conjunction with isotropic magnetic structures. In NVO it remains to be determined which scenario is the dominant one.

ACKNOWLEDGMENTS

This work was supported in part by the Israel US Binational Science Foundation under Grant No. 2000073. We thank C. Broholm for providing us the NVO powder samples used in this study.

APPENDIX A: FURTHER NEIGHBOR INTERACTIONS

1. Next-nearest neighbor spine interactions

We first consider next-nearest neighbor (NNN) interactions between spins on a given spine line. Since only the gradients with respect to Q_{y_p} are needed, we only consider those here. We set

$$\frac{\partial J_{\alpha\beta}(1,1')}{\partial Q_{y_p}} = V^{y_p}_{\alpha\beta}.$$

In what follows the index p will be left implicit. The operation 2_y takes this bond into itself with reversed indices. So, taking account of the transformation properties of Q_y, we require that

$$2_y \mathbf{V}^y = \tilde{\mathbf{V}}^y,$$

where 2_y is the twofold rotation operator. In terms of matrices, this relation is

$$2_y \mathbf{V}^y 2_y = \tilde{\mathbf{V}}^y,$$

where $2_y = \boldsymbol{\sigma}_x \boldsymbol{\sigma}_z$. Thus

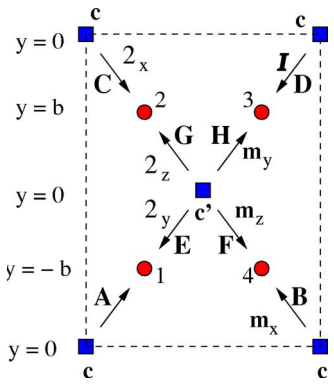

FIG. 11. (Color online) As Fig. 8. The eight different nearest-neighbor spine-cross tie interactions are labeled $A\cdots H$. The arrow points from the first site index to the second site index. We also give the symmetry operation one has to apply to interaction A to get each of the other interactions.

$$\mathbf{V}^y = \begin{bmatrix} K^y_{xx} & E^y_z & K^y_{xz} \\ -E^y_z & K^y_{yy} & E^y_x \\ K^y_{xz} & -E^y_x & K^y_{zz} \end{bmatrix}.$$

Likewise we have that

$$\frac{\partial J_{\alpha\beta}(2,2')}{\partial Q_y} = -2_x \mathbf{V}^y 2_x = \begin{bmatrix} -K^y_{xx} & E^y_z & K^y_{xz} \\ -E^y_z & -K^y_{yy} & -E^y_x \\ K_{xz} & E^y_x & -K^y_{zz} \end{bmatrix},$$

$$\frac{\partial J_{\alpha\beta}(3',3)}{\partial Q_y} = -\boldsymbol{\sigma}_y \mathbf{V}^y \boldsymbol{\sigma}_y = \begin{bmatrix} -K^y_{xx} & E^y_z & -K^y_{xz} \\ -E^y_z & -K^y_{yy} & E^y_x \\ -K^y_{xz} & -E^y_x & -K^y_{zz} \end{bmatrix},$$

$$\frac{\partial J_{\alpha\beta}(4',4)}{\partial Q_y} = \boldsymbol{\sigma}_x \tilde{\mathbf{V}}^y \boldsymbol{\sigma}_x = \begin{bmatrix} K^y_{xx} & E^y_z & -K^y_{xz} \\ -E^y_z & K^y_{yy} & -E^y_x \\ -K^y_{xz} & E^y_x & K^y_{zz} \end{bmatrix}.$$

2. Spine cross-tie interactions

In this section we analyze the spine-cross tie interactions, shown in Fig. 11, again keeping only derivative with respect to Q_{y_p} (here denoted Q_y). We set the interaction of type A to be

$$\frac{\partial J_{\alpha\beta}(c,1)}{dQ_y} = W^y_{\alpha\beta},$$

where

$$\mathbf{W}^y = \begin{bmatrix} L^y_{xx} & L^y_{xy} + F^y_z & L^y_{xz} - F^y_y \\ L^y_{xy} - F^y_z & L^y_{yy} & L^y_{yz} + F^y_x \\ L^y_{xz} + F^y_y & L^y_{yz} - F^y_x & L^y_{zz} \end{bmatrix}.$$

Also

$$\frac{\partial \mathbf{J}(c,4)}{\partial Q_y} = \boldsymbol{\sigma}_x \mathbf{W}^y \boldsymbol{\sigma}_x = \begin{bmatrix} L^y_{xx} & -L^y_{xy} - F^y_z & -L^y_{xz} + F^y_y \\ -L^y_{xy} + F^y_z & L^y_{yy} & L^y_{yz} + F^y_x \\ -L^y_{xz} - F^y_y & L^y_{yz} - F^y_x & L^y_{zz} \end{bmatrix},$$

$$\frac{\partial \mathbf{J}(c,2)}{\partial Q_y} = -2_x \mathbf{W}^y 2_x = \begin{bmatrix} -L^y_{xx} & L^y_{xy} + F^y_z & L^y_{xz} - F^u_y \\ L^y_{xy} - F^y_z & -L^y_{yy} & -L^y_{yz} - F^y_x \\ L^y_{xz} + F^y_y & -L^y_{yz} + F^y_x & -L^y_{zz} \end{bmatrix},$$

$$\frac{\partial \mathbf{J}(c,3)}{\partial Q_y} = -\mathcal{I}\mathbf{W}^y \mathcal{I} = \begin{bmatrix} -L^y_{xx} & -L^y_{xy} - F^y_z & -L^y_{xz} + F^y_y \\ -L^y_{xy} + F^y_z & -L^y_{yy} & -L^y_{yz} - F^y_x \\ -L^y_{xz} - F^y_y & -L^y_{yz} + F^y_x & -L^y_{zz} \end{bmatrix},$$

$$\frac{\partial \mathbf{J}(c',1)}{\partial Q_y} = 2_y \mathbf{W}^y 2_y = \begin{bmatrix} L^y_{xx} & -L^y_{xy} - F^y_z & L^y_{xz} - F^y_y \\ -L^y_{xy} + F^y_z & L^y_{yy} & -L^y_{yz} - F^y_x \\ L^y_{xz} + F^y_y & -L^y_{yz} + F^y_x & L^y_{zz} \end{bmatrix},$$

$$\frac{\partial \mathbf{J}(c',4)}{\partial Q_y} = \boldsymbol{\sigma}_z \mathbf{W}^y \boldsymbol{\sigma}_z = \begin{bmatrix} L^y_{xx} & L^y_{xy} + F^y_z & -L^y_{xz} + F^y_y \\ L^y_{xy} - F^y_z & L^y_{yy} & -L^y_{yz} - F^y_x \\ -L^y_{xz} - F^y_y & -L^y_{yz} + F^y_x & L^y_{zz} \end{bmatrix},$$

$$\frac{\partial \mathbf{J}(c',2)}{\partial Q_y} = -2_z \mathbf{W}^y 2_z = \begin{bmatrix} -L^y_{xx} & -L^y_{xy} - F^y_z & L^y_{xz} - F^y_y \\ -L^y_{xy} + F^y_z & -L^y_{yy} & L^y_{yz} + F^y_x \\ L^y_{xz} + F^y_y & L^y_{yz} - F^y_x & -L^y_{zz} \end{bmatrix}.$$

$$\frac{\partial \mathbf{J}(c',3)}{\partial Q_y} = -\boldsymbol{\sigma}_y \mathbf{W}^y \boldsymbol{\sigma}_y = \begin{bmatrix} -L^y_{xx} & L^y_{xy} + F^y_z & -L^y_{xz} + F^y_y \\ L^y_{xy} - F^y_z & -L^y_{yy} & L^y_{yz} + F^y_x \\ -L^y_{xz} - F^y_y & L^y_{yz} - F^y_x & -L^y_{zz} \end{bmatrix}.$$

APPENDIX B: SPIN-PHONON INTERACTION

In this Appendix $V_\alpha(X)$ denotes terms in the spin phonon interaction proportional to $Q_{\alpha_p} X$, where X is the phonon derivative of an exchange coefficient and the index p will be left implicit. We replace the spin operators by their values in Eq. (2).

1. NN spine interactions

We have

$$V_y(J^y_{xx}) = Q_y J^y_{xx} \sum [S_x(1)S_x(4) - S_x(2)S_x(3) + S_x(4)S_x(1') - S_x(3)S_x(2')] = -16 N_{uc} Q_y J^y_{xx} \cos(qa/2) \mathfrak{I}[a_x b^*_x],$$

where the sum is over the N_{uc} unit cells, $x_{14}=x_1-x_4$, and $\mathbf{S}(n)$ denotes a spin on sublattice n, as in Fig. 1. Similar algebra then yields the other relevant interactions

$$V_y(J^y_{yy}) = Q_y J^y_{yy} \sum [S_y(1)S_y(4) - S_y(2)S_y(3) + S_y(4)S_y(1') - S_y(3)S_y(2')] = 16 N_{uc} Q_y J^y_{yy} \cos(qa/2) \mathfrak{I}[a_y b^*_y],$$

$$V_y(J^y_{zz}) = Q_y J^y_{zz} \sum [S_z(1)S_z(4) - S_z(2)S_z(3) + S_z(4)S_z(1') - S_z(3)S_z(2')] = 16 N_{uc} Q_y J^y_{zz} \cos(qa/2) \mathfrak{I}[a_z b^*_z],$$

$$V_y(J^y_{yz}) = Q_y J^y_{yz} \sum [S_y(1)S_z(4) + S_z(1)S_y(4) - S_z(2)S_y(3) - S_y(2)S_z(3) - S_y(4)S_z(1') - S_z(4)S_y(1') + S_y(3)S_z(2') + S_z(3)S_y(2')] = -16 N_{uc} Q_y \sin(qa/2) J^y_{yz} \mathfrak{I}[a^*_y b_z + b^*_y a_z],$$

$$V_y(D^y_z) = Q_y D^y_z \sum [S_x(1)S_y(4) - S_y(1)S_x(4) + S_x(2)S_y(3) - S_y(2)S_x(3) + S_x(4)S_y(1') - S_y(4)S_x(1') + S_x(3)S_y(2') - S_y(3)S_x(2')] = -16 N_{uc} Q_y \sin(qa/2) D^y_z \mathfrak{I}[a^*_y b_x + b^*_y a_x],$$

$$V_y(D^y_y) = Q_y D^y_y \sum [-S_x(1)S_z(4) + S_z(1)S_x(4) - S_x(2)S_z(3) + S_z(2)S_x(3) + S_x(4)S_z(1') - S_z(4)S_x(1') + S_x(3)S_z(2') - S_z(3)S_x(2')] = -16 N_{uc} Q_y \cos(qa/2) D^y_y \mathfrak{I}[a_x b^*_z + b^*_x a_z].$$

2. NNN spine interactions

Now we analyze the NNN spine interactions. We have

$$V_y(K^y_{xx}) = Q_y K^y_{xx} \sum [S_x(1)S_x(1') - S_x(2)S_x(2') - S_x(3)S_x(3') + S_x(4)S_x(4')] = 16 N_{uc} Q_y K^y_{xx} \cos(qa) \mathfrak{I}[a_{s,x} b^*_{s,x}].$$

Similarly,

$$V_y(K^y_{yy}) = Q_y K^y_{yy} \sum [S_y(1)S_y(1') - S_y(2)S_y(2') - S_y(3)S_y(3') + S_y(4)S_y(4')] = 16 N_{uc} Q_y K^y_{yy} \cos(qa) \mathfrak{I}[a^*_{s,y} b_{s,y}],$$

$$V_y(K^y_{zz}) = Q_y K^y_{zz} \sum (S_z(1)S_z(1') - S_z(2)S_z(2') - S_z(3)S_z(3') + S_z(4)S_z(4')) = 16 N_{uc} Q_y K^y_{zz} \cos(qa) \mathfrak{I}[a_{s,z} b^*_{s,z}],$$

$$V_y(E^y_z) = Q_y E^y_z \sum [S_x(1)S_y(1') - S_y(1)S_x(1') + S_x(2)S_y(2') - S_y(2)S_x(2') + S_x(3')S_y(3) - S_y(3')S_x(3) + S_x(4')S_y(4) - S_y(4')S_x(4)] = 16 N_{uc} Q_y E^y_z \sin(qa) \mathfrak{I}[a_{s,x} b^*_{s,y} + b_{s,x} a^*_{s,y}],$$

$$V_y(E^y_x) = Q_y E^y_x \sum [S_y(1)S_z(1') - S_z(1)S_y(1') - S_y(2)S_z(2') + S_z(2)S_y(2') + S_y(3')S_z(3) - S_z(3')S_y(3) - S_y(4')S_z(4) + S_z(4')S_y(4)] = 16 N_{uc} Q_y E^y_x \sin(qa) \mathfrak{I}[a_{s,y} b^*_{s,z} + b_{s,y} a^*_{s,z}],$$

$$V_y(K^y_{xz}) = Q_y K^y_{xz} \sum [S_x(1)S_z(1') + S_z(1)S_x(1') + S_x(2)S_z(2') + S_z(2)S_x(2') - S_x(3)S_z(3') - S_z(3)S_x(3') - S_x(4)S_z(4') - S_z(4)S_x(4')] = 16 N_{uc} Q_y K^y_{xz} \cos(qa) \mathfrak{I}[a_{s,x} b^*_{s,z} + a_{s,z} b^*_{s,x}].$$

3. Spine cross-tie interactions

Now we analyze the spine cross-tie interactions

$$V_y(L^y_{xx}) = Q_y L^y_{xx} \sum [S_x(5) + S_x(6)][S_x(1) - S_x(2) - S_x(3) + S_x(4)] \equiv N_{uc} Q_y L^y_{xx}[u_{xx} + u^*_{xx}],$$

where

$$\begin{aligned} u_{xx} = b_{cx}[&(a^*_{s,x} - ib^*_{s,x})e^{-iqa/4} - (a^*_{s,x} + ib^*_{s,x})e^{iqa/4} - (-a^*_{s,x} \\ &- ib^*_{s,x})e^{-iqa/4} + (-a^*_{s,x} + ib^*_{s,x})e^{iqa/4} - (a^*_{s,x} - ib^*_{s,x})e^{iqa/4} \\ &+ (-a^*_{s,x} - ib^*_{s,x})e^{iqa/4} + (a^*_{s,x} + ib^*_{s,x})e^{-iqa/4} \\ &- (-a^*_{s,x} + ib^*_{s,x})e^{-iqa/4}] \end{aligned}$$

so that

$$V_y(L^y_{xx}) = 16 N_{uc} Q_y L^y_{xx} \sin(qa/4) \Im[b_{cx} a^*_{s,x}].$$

Similarly

$$\begin{aligned} V_y(L^y_{yy}) &= Q_y L^y_{yy} \sum [S_y(5) + S_y(6)] \\ &\quad \times [S_y(1) - S_y(2) - S_y(3) + S_y(4)] \\ &= 16 N_{uc} Q_y L^y_{yy} \sin(qa/4) \Im[a_{cy} b^*_{s,y}], \end{aligned}$$

$$\begin{aligned} V_y(L^y_{zz}) &= Q_y L^y_{zz} \sum [S_z(5) + S_z(6)] \\ &\quad \times [S_z(1) - S_z(2) - S_z(3) + S_z(4)] \\ &= 16 N_{uc} Q_y L^y_{zz} \cos(qa/4) \Im[a_{cz} b^*_{s,z}], \end{aligned}$$

$$\begin{aligned} V_y(L^y_{xy}) &= Q_y L^y_{xy} \sum ([S_y(1) + S_y(2) - S_y(3) - S_y(4)] \\ &\quad \times [S_x(5) - S_x(6)] + [S_y(5) - S_y(6)] \\ &\quad \times [S_x(1) + S_x(2) - S_x(3) - S_x(4)]) \\ &= 16 N_{uc} Q_y L^y_{xy} \cos(qa/4) \Im[b_{cx} a^*_{s,y} + a_{cy} b^*_{s,x}], \end{aligned}$$

$$\begin{aligned} V_y(L^y_{xz}) &= Q_y L^y_{xz} \sum ([S_z(1) + S_z(2) - S_z(3) - S_z(4)] \\ &\quad \times [S_x(5) + S_x(6)] + [S_z(5) + S_z(6)] \\ &\quad \times [S_x(1) + S_x(2) - S_x(3) - S_x(4)]) \\ &= 16 N_{uc} Q_y L^y_{xz} (\sin(qa/4) \Im[b_{cx} a^*_{s,z}] \\ &\quad + \cos(qa/4) \Im[a_{cz} b^*_{s,x}]), \end{aligned}$$

$$\begin{aligned} V_y(L^y_{yz}) &= Q_y L^y_{yz} \sum ([S_z(1) - S_z(2) - S_z(3) + S_z(4)] \\ &\quad \times [S_y(5) - S_y(6)] + [S_z(5) - S_z(6)] \\ &\quad \times [S_y(1) - S_y(2) - S_y(3) + S_y(4)]) \\ &= 16 N_{uc} Q_y L^y_{yz} (\cos(qa/4) \Im[a_{cy} b^*_{s,z}] \\ &\quad + \sin(qa/4) \Im[a_{cz} b^*_{s,y}]), \end{aligned}$$

$$\begin{aligned} V_y(F^y_x) &= Q_y F^y_x \sum ([S_z(1) - S_z(2) - S_z(3) + S_z(4)] \\ &\quad \times [S_y(5) - S_y(6)] - [S_z(5) - S_z(6)] \\ &\quad \times [S_y(1) - S_y(2) - S_y(3) + S_y(4)]) \\ &= 16 N_{uc} Q_y F^y_x (\cos(qa/4) \Im[a_{cy} b^*_{s,z}] \\ &\quad + \sin(qa/4) \Im[a^*_{cz} b_{s,y}]), \end{aligned}$$

$$\begin{aligned} V_y(F^y_y) &= Q_y F^y_y \sum (-[S_z(1) + S_z(2) - S_z(3) - S_z(4)] \\ &\quad \times [S_x(5) + S_x(6)] + [S_z(5) + S_z(6)] \\ &\quad \times [S_x(1) + S_x(2) - S_x(3) - S_x(4)]) \\ &= 16 N_{uc} Q_y F^y_y (\sin(qa/4) \Im[b^*_{cx} a_{s,z}] \\ &\quad + \cos(aq/4) \Im[a_{cz} b^*_{s,x}]), \end{aligned}$$

$$\begin{aligned} V_y(F^y_z) &= Q_y F^y_z \sum ([S_y(1) + S_y(2) - S_y(3) - S_y(4)] \\ &\quad \times [S_x(5) - S_x(6)] - [S_y(5) - S_y(6)] \\ &\quad \times [S_x(1) + S_x(2) - S_x(3) - S_x(4)]) \\ &= 16 N_{uc} Q_y F^y_z \cos(qa/4) \Im[b_{cx} a^*_{s,y} + a^*_{cy} b_{s,x}]. \end{aligned} \tag{B1}$$

[1] N. Rogado, G. Lawes, D. A. Huse, A. P. Ramirez, and R. J. Cava, Solid State Commun. **124**, 229 (2002).

[2] G. Lawes, M. Kenzelmann, N. Rogado, K. H. Kim, G. A. Jorge, R. J. Cava, A. Aharony, O. Entin-Wohlman, A. B. Harris, T. Yildirim, Q. Z. Huang, S. Park, C. Broholm, and A. P. Ramirez, Phys. Rev. Lett. **93**, 247201 (2004).

[3] G. Lawes, A. B. Harris, T. Kimura, N. Rogado, R. J. Cava, A. Aharony, O. Entin-Wohlman, T. Yildirim, M. Kenzelmann, C. Broholm, and A. P. Ramirez, Phys. Rev. Lett. **95**, 087205 (2005).

[4] M. Kenzelmann, A. B. Harris, A. Aharony, O. Entin-Wohlman, T. Yildirim, Q. Huang, S. Park, G. Lawes, C. Broholm, N. Rogado, R. J. Cava, K. H. Kim, G. Jorge, and A. P. Ramirez, cond-mat/0510386 (unpublished).

[5] N. Hur, S. Park, P. A. Sharma, J. S. Ahn, S. Guha, and S.-W. Cheong, Nature (London) **429**, 392 (2004).

[6] M. Kenzelmann, A. B. Harris, S. Jonas, C. Broholm, J. Schefer, S. B. Kim, C. L. Zhang, S.-W. Cheong, O. P. Vajk, and J. W. Lynn, Phys. Rev. Lett. **95**, 087206 (2005).

[7] A. B. Harris and G. Lawes, *Ferroelectricity in Incommensurate Magnets*, in *Handbook of Magnetism and Advanced Magnetic Materials* (J. Wiley, London, 2006); cond-mat/0508617 (unpublished); A. B. Harris, cond-mat/0508730 (unpublished).

[8] I. Dzyaloshinskii, J. Phys. Chem. Solids **4**, 241 (1958).

[9] T. Moriya, Phys. Rev. **120**, 91 (1960).
[10] I. A. Sergienko and E. Dagotto, Phys. Rev. B **73**, 094434 (2006).
[11] A. J. C. Wilson, *International Tables For Crystallography* (Kluwer Academic Publishers, Dordrecht, 1995), Vol. A.
[12] E. E. Sauerbrei, F. Faggiani, and C. Calvo, Acta Crystallogr. **29**, 2304 (1973).
[13] A. B. Harris, A. Aharony, O. Entin-Wohlman, T. Yildirim, and M. Kenzelmann (unpublished).
[14] J. R. D. Copley, D. A. Neumann, W. A. Kamitakahara, Can. J. Phys. **73**, 763 (1995).
[15] S. Baroni, A. Dal Corso, S. de Gironcoli, and P. Giannozzi, http://www.pwscf.org
[16] T. Yildirim, Chem. Phys. **261**, 205 (2000).
[17] E. P. Wigner, *Group Theory* (Academic Press, New York, 1959); M. Tinkham, *Group Theory and Quantum Mechanics* (McGraw-Hill, New York, 1964).
[18] Since the GD's give the relative amplitudes within a given Wyckoff orbit, the $O^n_{\tau,\alpha}$ for sites not listed in this table are those for the relevant GD. For motion in the y direction, the amplitude of all atoms is the same, i.e., that of the GD's we called y_1-y_6. For the displacements in the x and z directions the relative amplitudes are those of GD's y_7-y_{12} shown in Figs. 3–5.
[19] M. D. Segall, R. Shah, C. J. Pickard, and M. C. Payne, Phys. Rev. B **54**, 16317 (1996).
[20] Animations of the B_{2u} phonons can be found at http://www.ncnr.nist.gov/staff/taner/nvo
[21] P. C. Hohenberg and W. Kohn, Phys. Rev. **136**, B864 (1964); W. Kohn and L. J. Sham, Phys. Rev. **140**, A1133 (1965).
[22] V. I. Anisimov, F. Aryasetiawan, and A. I. Lichtenstein, J. Phys.: Condens. Matter **9**, 767 (1997).